

Charged Higgs boson in MSSM and beyond

Yaşar Hiçyılmaz,^{1,*} Levent Selbuz,^{2,†} Levent Solmaz,^{1,‡} and Cem Salih Ün^{3,§}

¹*Department of Physics, Balıkesir University, TR10145, Balıkesir, Turkey*

²*Department of Engineering Physics, Ankara University, TR06100, Ankara, Turkey*

³*Department of Physics, Uludağ University, 16059, Bursa, Turkey*



(Received 27 November 2017; revised manuscript received 5 May 2018; published 27 June 2018)

We conduct a numerical study over the constrained MSSM (CMSSM), next-to-MSSM (NMSSM) and $U(1)$ extended MSSM (UMSSM) to probe the allowed mass ranges of the charged Higgs boson and its dominant decay patterns, which might come into prominence in the near future collider experiments. We present results obtained from a limited scan for CMSSM as a basis and compare its predictions with the extended models. We observe within our data that a wide mass range is allowed as $0.5(1) \lesssim m_{H^\pm} \lesssim 17$ TeV in UMSSM (NMSSM). We find that the dominant decay channel is mostly $H^\pm \rightarrow tb$ such that $\text{BR}(H^\pm \rightarrow tb) \sim 80\%$. While this mode remains dominant over the whole allowed parameter space of CMSSM, we realize some special domains in the NMSSM and UMSSM, in which $\text{BR}(H^\pm \rightarrow tb) \lesssim 10\%$. In this context, the decay patterns of the charged Higgs can play a significant role to distinguish among the SUSY models. In addition to the tb decay mode, we find that the narrow mass scale in CMSSM allows only the decay modes for the charged Higgs boson to $\tau\nu$ ($\sim 16\%$), and their supersymmetric partners $\tilde{\tau}\tilde{\nu}$ ($\sim 13\%$). On the other hand, it is possible to realize the mode in NMSSM and UMSSM in which the charged Higgs boson decays into a chargino and neutralino pair up to about 25%. This decay mode requires nonuniversal boundary conditions within the MSSM framework to be available, since CMSSM yields $\text{BR}(H^\pm \rightarrow \tilde{\chi}_1^0\tilde{\chi}_1^\pm) \lesssim 1\%$. It can also be probed in the near future collider experiments through the missing energy and CP -violation measurements. Moreover, the chargino mass is realized as $m_{\tilde{\chi}_1^\pm} \gtrsim 1$ TeV in NMSSM and UMSSM, and these solutions will be likely tested soon in collider experiments through the chargino-neutralino production. Focusing on the chargino-neutralino decay patterns, we also present tables which list the possible ranges for the charged Higgs production and decay modes.

DOI: [10.1103/PhysRevD.97.115041](https://doi.org/10.1103/PhysRevD.97.115041)

I. INTRODUCTION

After the null results for the new physics, the current experiments have focused on the Higgs boson properties and analyses have been quite enlarged such that the Higgs boson couplings and decays are now being studied precisely. The Higgs boson itself is a strong hint for the new physics and there are some drawbacks of the Standard Model (SM) such as the gauge hierarchy problem [1] and the absolute stability of the SM Higgs potential [2]. In addition, most of the models beyond the SM (BSM) need to enlarge the Higgs sector so that their low scale

phenomenology includes extra Higgs bosons which are not present in the SM. Among many well motivated BSM models, supersymmetric models take arguably a special place, since they are able to solve the gauge hierarchy problem, provide plausible candidates for the dark matter (DM) and so on. Besides, the Higgs sector in such models requires two Higgs doublets and so the low scale Higgs sector includes two CP -even Higgs bosons (h, H), one CP -odd Higgs boson (A) and two charged Higgs bosons (H^\pm).

While the lightest CP -even Higgs boson is expected to exhibit very similar properties to the SM-like Higgs boson at the decoupling limit ($m_H \sim m_A \sim m_{H^\pm} \gg m_h$), its couplings to the SM particles can still deviate from the SM and, thus, it can be constrained by such deviations [3]. Similarly, the heavier Higgs bosons can be constrained if they can significantly decay into the SM particles. For instance, if the CP -odd Higgs boson decays mostly into a pair of τ leptons, then its mass can be constrained as $m_A \gtrsim 1$ TeV depending on $\tan\beta$ [4]. In addition, the flavor changing decays of the B meson also yield important implications for these Higgs bosons. The $B_s \rightarrow \mu^+\mu^-$ process receives some

* yasarhicilyilmaz@balikesir.edu.tr

† selbuz@eng.ankara.edu.tr

‡ lsolmaz@balikesir.edu.tr

§ cemsalihun@uludag.edu.tr

Published by the American Physical Society under the terms of the [Creative Commons Attribution 4.0 International license](https://creativecommons.org/licenses/by/4.0/). Further distribution of this work must maintain attribution to the author(s) and the published article's title, journal citation, and DOI. Funded by SCOAP³.

contributions from the A boson proportional to $(\tan\beta)^6/m_A^4$ [5], and the strong agreement between the experimental results ($\text{BR}(B_s \rightarrow \mu^+\mu^-) = 3.2_{-1.2}^{+1.5} \times 10^{-9}$ [6]) and the SM ($\text{BR}(B_s \rightarrow \mu^+\mu^-) = (3.2 \pm 0.2) \times 10^{-9}$ [7]) strictly constrains the A -boson phenomenology.

Among these extra Higgs bosons, the charged Higgs boson plays a crucial role, since the SM does not have any charged scalar. It can be produced at the current collider experiments along with other particles as $pp \rightarrow (t, W^\pm, t\bar{b}, \dots)H^\pm$, where p stands for the proton. Even though its production is rather difficult and the production cross section is small in comparison to the other particles, the charged Higgs boson can be visible with large center of mass energy and luminosity in near future collider experiments. In this context, the track of its decays can be directly related to the new physics. Furthermore, this distinguishing charged particle may reveal itself in many manifestations and different supersymmetric models may favor different predictions. Even though the usual dominant decay mode is $H^\pm \rightarrow t\bar{b}$ when $m_{H^\pm} \gtrsim m_t + m_b$ in the constrained MSSM (CMSSM), models with extended particle content and/or gauge group can open the window for other probable and important decay modes. In addition, richer phenomenology can be revealed when the charged Higgs boson is allowed to decay into new supersymmetric particles. For instance, if the $H^\pm \rightarrow \tilde{\chi}_i^0 \tilde{\chi}_j^\pm$ mode is open, one can also measure the CP asymmetry throughout such processes [8].

Based on different decay patterns of the charged Higgs boson, we analyzed the charged Higgs boson in this work within three different models which are the minimal supersymmetric extension of the SM (MSSM), $U(1)$ extended MSSM (UMSSM) and next-to-MSSM (NMSSM). We restrict our analyses to constrained versions of these models, in which the low scale observables can be determined with only a few input parameters defined at the grand unification scale (M_{GUT}). Of course, a more detailed study can be performed from the weak scale side which is a tedious work and this is beyond the scope of this paper. Throughout the analyses the CMSSM framework will be considered as the base and implications of the other two models will be discussed in a way that also compares them with CMSSM. It is important to stress that the different imprints of the charged Higgs boson can be used to distinguish a model from another and this may be useful for future charged Higgs studies.

The outline of the rest of the paper is the following: We will briefly describe the models under concern in Sec. II. After we summarize the scanning procedure, employed experimental constraints in Secs. III and IV discusses the mass spectrum in terms of the particles, which can participate in the charged Higgs boson decay modes. The results for the production and decay modes of the charged Higgs boson are presented in Sec. V. We also present tables containing rates for the charged Higgs boson production and its decay modes over some benchmark

points in this section. Section VI summarizes and concludes our findings.

II. MODELS

A. MSSM

The superpotential in MSSM is given as

$$W_{\text{MSSM}} = \mu \hat{H}_u \hat{H}_d + Y_u \hat{Q} \hat{H}_u \hat{U} + Y_d \hat{Q} \hat{H}_d \hat{D} + Y_e \hat{L} \hat{H}_d \hat{E}, \quad (1)$$

where μ is the bilinear mixing term for the MSSM Higgs doublets H_u and H_d ; Q and L denote the left-handed squark and lepton doublets, while U , D , E stand for the right-handed u-type squarks, d-type squarks and sleptons, respectively. $Y_{u,d,e}$ are the Yukawa couplings between the Higgs fields and the matter fields shown as subscripts. The Higgsino mass term μ is included in the SUSY preserving Lagrangian in MSSM, and hence it is allowed to be at any scale from the electroweak (EW) scale to M_{GUT} . In this sense, even though it is relevant to the EW symmetry breaking, its scale is not constrained by the EW symmetry breaking scale (~ 100 GeV). This is called the μ problem in MSSM. In addition to W_{MSSM} , the soft SUSY breaking (SSB) Lagrangian is given below:

$$\begin{aligned} -\mathcal{L}_{\text{MSSM}}^{\text{SSB}} = & m_{H_u}^2 |H_u|^2 + m_{H_d}^2 |H_d|^2 + m_{\tilde{Q}}^2 |\tilde{Q}|^2 + m_{\tilde{L}}^2 |\tilde{L}|^2 \\ & + m_{\tilde{U}}^2 |\tilde{U}|^2 + m_{\tilde{D}}^2 |\tilde{D}|^2 + m_{\tilde{E}}^2 |\tilde{E}|^2 \\ & + \sum_a M_a \lambda_a \lambda_a + (B\mu H_u H_d + \text{H.c.}) \\ & + A_u Y_u \tilde{Q} H_u \tilde{U}^c + A_d Y_d \tilde{Q} H_d \tilde{D}^c \\ & + A_e Y_e \tilde{L} H_d \tilde{E}^c \end{aligned} \quad (2)$$

where the field notation is as given before. In addition, m_ϕ^2 with $\phi = H_u, H_d, \tilde{Q}, \tilde{L}, \tilde{U}, \tilde{D}, \tilde{E}$ are the SSB mass terms for the scalar fields. $A_{u,d,e}$ are the SSB terms for the trilinear scalar interactions, while B is the SSB bilinear mixing term for the MSSM Higgs fields. After adding the SSB Lagrangian, the Higgs potential in MSSM becomes more complicated than the SM, and the masses of the physical Higgs bosons can be found in terms of μ , m_{H_u} , m_{H_d} and $\tan\beta$, where $\tan\beta = v_u/v_d$ is the ratio of the vacuum expectation values (VEVs) of the MSSM Higgs fields. The tree level Higgs boson masses can be found as [9]

$$\begin{aligned} m_{h,H} &= \frac{1}{2} \left(m_A^2 + M_Z^2 \mp \sqrt{(m_A^2 - M_Z^2)^2 + 4M_Z^2 m_A^2 \sin^2(2\beta)} \right) \\ m_{H^\pm}^2 &= m_A^2 + M_W^2 \\ m_A^2 &= 2|\mu|^2 + m_{H_u}^2 + m_{H_d}^2, \end{aligned} \quad (3)$$

where M_Z and M_W are the masses of the Z and W bosons, respectively. As it is well known, the lightest CP -even

Higgs boson tree level mass is problematic in MSSM, since it is bounded by M_Z from above as $m_h^2 \lesssim M_Z^2 \cos^2(2\beta)$. This conflict can be resolved by adding the loop corrections to the Higgs boson mass. Utilizing the loop corrections to realize the 125 GeV Higgs boson at the low scale requires either multi-TeV stop mass or relatively large SSB trilinear A term [10]. In this context the 125 GeV Higgs boson constraint leads to a heavy spectrum in SUSY particles especially in the CMSSM framework where all scalar masses are set by a single parameter at M_{GUT} . Besides, if the mass scales for the extra Higgs bosons are realized as $m_A \sim m_H \sim m_{H^\pm} \gtrsim 1$ TeV, it requires large m_{H_u} and m_{H_d} as seen from Eq. (3). It also brings the naturalness problem back to the SUSY models, since the consistent electroweak symmetry breaking scale requires $\mu \approx m_{H_u}$ over most of the fundamental parameter space of the models. It also arises the μ problem in the MSSM mentioned above.

The μ term is also important since it is the Higgsino masses at the low scale. In this context, if the μ term is significantly low in comparison to the gaugino masses M_1 and M_2 , the lightest supersymmetric particle (LSP) neutralino can exhibit Higgsino-like properties, and it yields different DM phenomenology. The nature of the DM can be investigated by considering the neutralino mass matrix given as

$$\mathcal{M}_{\tilde{\chi}^0}^{\text{MSSM}} = \begin{pmatrix} M_1 & 0 & -\frac{g_1 v_d}{\sqrt{2}} & \frac{g_1 v_u}{\sqrt{2}} \\ 0 & M_2 & \frac{g_2 v_d}{\sqrt{2}} & -\frac{g_2 v_u}{\sqrt{2}} \\ -\frac{g_1 v_d}{\sqrt{2}} & \frac{g_2 v_d}{\sqrt{2}} & 0 & -\mu \\ \frac{g_1 v_u}{\sqrt{2}} & -\frac{g_2 v_u}{\sqrt{2}} & -\mu & 0 \end{pmatrix} \quad (4)$$

in the basis $(\tilde{B}, \tilde{W}, \tilde{h}_d, \tilde{h}_u)$, where \tilde{B} and \tilde{W} denote Bino and Wino respectively, which may be called electroweakinos, while \tilde{h}_d and \tilde{h}_u represent the Higgsinos from H_d and H_u superfields respectively. Similarly, the chargino mass matrix can be written as

$$\mathcal{M}_{\tilde{\chi}^\pm} = \begin{pmatrix} M_2 & \frac{1}{\sqrt{2}} g_2 v_u \\ \frac{1}{\sqrt{2}} g_2 v_d & \mu \end{pmatrix}. \quad (5)$$

The properties and relevant phenomenology involving with the chargino and neutralino can be understood by comparing M_1 , M_2 and μ . If $\mu > M_1, M_2$ then both LSP neutralino and the lightest chargino exhibit gaugino properties and the gauge couplings are dominant in the strength of the relevant interactions. When $\mu < M_1, M_2$, the LSP neutralino and the lightest chargino are mostly formed by the Higgsinos, and the Yukawa couplings also take part in interactions as well as the gauge couplings. Since the charged Higgs is, in principle, allowed to decay into a pair of a neutralino and a chargino, the self-interaction couplings in the Higgs sector are also important in such

decay processes, when the chargino and neutralino are Higgsino-like.

B. NMSSM

The main idea behind NMSSM is to resolve the μ problem of MSSM in a dynamic way that an additional S field generates the μ term by developing a nonzero VEV. It can be realized by replacing the term with the μ term in W_{MSSM} given in Eq. (1) with a trilinear term as $h_s S H_u H_d$, where S is chosen preferably to be singlet under the MSSM gauge group. If there is no additional term depending on the S field, then the Lagrangian also remains invariant under Pecce-Quinn (PQ) like symmetry which transforms the fields as follows:

$$\begin{aligned} H_u &\rightarrow e^{iq_{PQ}\theta} H_u & H_d &\rightarrow e^{iq_{PQ}\theta} H_d & S &\rightarrow e^{-2iq_{PQ}\theta} \\ Q &\rightarrow e^{-iq_{PQ}\theta} Q & L &\rightarrow e^{-iq_{PQ}\theta} L & U, D, E &\rightarrow U, D, E. \end{aligned} \quad (6)$$

Such a symmetry in the Lagrangian can help to resolve the strong CP problem [11]. However, in NMSSM, the Pecce-Quinn symmetry is broken by the μ term spontaneously, since it happens by the VEV of the S field. In this case, there has to be a massless Goldstone boson, which can be identified as axion. Such a massless field is strongly constrained by the cosmological observations [12]. Moreover, h_s is restricted into a very narrow range ($10^{-10} \gtrsim h_s \lesssim 10^{-7}$) experimentally, and in order to yield $\mu \sim \mathcal{O}(100)$ GeV VEV of S should be very large, and it brings back the naturalness problem.

The situation of the massless Goldstone boson, arising from the spontaneous breaking of the PQ symmetry, can be avoided by adding another S dependent term as $\frac{1}{3}\kappa S^3$, which explicitly breaks the PQ symmetry, while \mathbb{Z}_3 symmetry remains unbroken. However, despite avoiding the massless axion in this case, the effectively generated μ term spontaneously breaks the discrete \mathbb{Z}_3 symmetry, which arises the domain-wall problem. This problem can be resolved by adding nonrenormalizable higher order operators which break \mathbb{Z}_3 symmetry, while preserving the \mathbb{Z}_2 symmetry at the Planck scale. (For a detailed description of the domain-wall problem and its resolution, see [13].) In our work we assume that the domain-wall problem is resolved and we consider the following superpotential in the NMSSM framework:

$$W_{\text{NMSSM}} = W_{\text{MSSM}}(\mu = 0) + h_s \hat{S} \hat{H}_u \hat{H}_d + \frac{1}{3} \kappa \hat{S}^3 \quad (7)$$

and the corresponding SSB Lagrangian is

$$\begin{aligned} \mathcal{L}_{\text{NMSSM}}^{\text{SUSY}} &= \mathcal{L}_{\text{MSSM}}^{\text{SUSY}}(\mu = 0) - m_S^2 S^* S \\ &\quad - \left[h_s A_s S H_u H_d + \frac{1}{3} \kappa A_\kappa S^3 + \text{H.c.} \right], \end{aligned} \quad (8)$$

where $\mathcal{L}_{\text{MSSM}}^{\text{SUSY}}(\mu = 0)$ is the SSB Lagrangian for MSSM given in Eq. (2) with $\mu = 0$, m_S is the mass for the scalar component of S , while A_s and A_χ are trilinear SSB terms for the scalar interactions. According to the superpotential and the SSB Lagrangian, the second term in Eq. (7) is responsible for generating the μ term effectively as $\mu_{\text{eff}} \equiv h_s v_s / \sqrt{2}$ and the first term in the parentheses of Eq. (8) is $B\mu$ correspondence. Although the particle content is simply enlarged by including an extra singlet field in NMSSM, the neutral scalar component of this field can mix with the CP -even and CP -odd Higgs boson of MSSM, while the charged Higgs sector remains intact. After the EW symmetry breaking, the NMSSM Higgs sector includes three CP -even Higgs bosons, two CP -odd Higgs bosons and two charged Higgs bosons. A detailed discussion for the Higgs sector can be found in Ref. [14]. Once the mass matrix for the CP -even Higgs boson states is diagonalized, the lightest mass eigenvalue can be found as

$$m_h^2 = M_Z \left(\cos^2(2\beta) + \frac{h_s}{g} \right), \quad (9)$$

where the first term covers the MSSM part of the Higgs boson, while the second term encodes the contributions to the tree-level Higgs boson mass from the singlet. In this sense, the necessary loop corrections to the Higgs boson mass may be relaxed and lighter mass spectrum for the SUSY particles can be realized. As the lightest CP -even Higgs boson, other Higgs bosons receive contributions from the singlet, and the tree-level mass for the charged Higgs boson can be obtained as [15]

$$m_{H^\pm}^2 = M_W^2 + \frac{2h_s v_s}{\sin(2\beta)} (A_s + \kappa v_s) - h_s (v_u^2 + v_d^2). \quad (10)$$

In addition to the Higgs sector, the neutralino sector of NMSSM has five neutralinos including to the supersymmetric partner of S field—so-called singlino—in addition to the MSSM neutralinos. The mass matrix for the neutralinos in the basis $(\tilde{B}, \tilde{W}, \tilde{H}_u, \tilde{H}_d, \tilde{S})$ is obtained as

$$\mathcal{M}_{\tilde{\chi}^0}^{\text{NMSSM}} = \left(\begin{array}{cccc|c} & & & & 0 \\ & & & & 0 \\ & \mathcal{M}_{\tilde{\chi}^0}^{\text{MSSM}}(\mu = \mu_{\text{eff}}) & & & -h_s v_u \\ \hline & & & & -h_s v_d \\ 0 & 0 & -h_s v_u & -h_s v_d & 2\kappa v_s \end{array} \right), \quad (11)$$

where $\mathcal{M}_{\tilde{\chi}^0}^{\text{MSSM}}(\mu = \mu_{\text{eff}})$ is the MSSM neutralino masses and mixing as given in Eq. (4), while the extra column and row represent the mixing of the singlino with the MSSM neutralinos. As seen from the $\mathcal{M}_{\tilde{\chi}^0}^{\text{SUSY}}$, the singlino mass is

found as $M_{\tilde{S}} = 2\kappa v_s$. Even though it is left out from the first 4×4 matrix of the MSSM neutralinos, the singlet sector is still effective, since the mass term for the Higgsinos is determined by the VEV of the S field as $\mu_{\text{eff}} = h_s v_s / \sqrt{2}$. If one assumes the lightest mass eigenvalue of $\mathcal{M}_{\tilde{\chi}^0}$ is also the lightest supersymmetric particle (LSP), species of the LSP can yield dramatically different dark matter (DM) implications than those obtained in the MSSM framework, especially when the singlino is realized so light that it can significantly mix with the other neutralinos in formation of the LSP neutralino. The chargino sector remains intact, since NMSSM does not introduce any new charged field to the particle content; hence, the chargino masses and mixing are given with the same matrix given in Eq. (5). Note that the VEV of the singlet field is indirectly effective in the chargino sector through the Higgsino mass, which can be seen by replacing μ with μ_{eff} in Eq. (5).

C. UMSSM

In the previous subsection, where we discussed NMSSM, even though its nonzero VEV might be expected to break a gauged symmetry spontaneously, there was no symmetry whose breaking is triggered with VEV of S except the global PQ and \mathbb{Z}_3 symmetries. In this sense, one can associate a gauged symmetry to v_s by extending the MSSM gauge group with a simple Abelian $U(1)'$ symmetry [16,17]. Such extensions of MSSM form a class of $U(1)'$ models (UMSSM), and its gauge structure can be originated to the grand unified theory (GUT) scale, when the underlying symmetry group at M_{GUT} is larger than $SU(5)$. The most interesting breaking pattern, which results in UMSSM, can be realized when the GUT symmetry is identified with the exceptional group E_6 :

$$\begin{aligned} E_6 &\rightarrow SO(10) \times U(1)_\psi \rightarrow SU(5) \times U(1)_\chi \times U(1)_\psi \\ &\rightarrow G_{\text{MSSM}} \times U(1)', \end{aligned} \quad (12)$$

where $G_{\text{MSSM}} = SU(3)_c \times SU(2)_L \times U(1)_Y$ is the MSSM gauge group, and $U(1)'$ can be expressed as a general mixing of $U(1)_\psi$ and $U(1)_\chi$ as

$$U(1)' = \cos\theta_{E_6} U(1)_\chi + \sin\theta_{E_6} U(1)_\psi. \quad (13)$$

In a general treatment, all the fields including the MSSM ones are allowed to have nonzero charges under the $U(1)'$ gauge group; thus, despite the similarity with NMSSM, the invariance under the $U(1)'$ symmetry does not allow the term κS^3 as well as $\mu H_u H_d$. The charge configurations of the fields for $U(1)_\psi$ and $U(1)_\chi$ models are given in Table I. The charge configuration for any $U(1)'$ model can be obtained with the mixing of $U(1)_\psi$ and $U(1)_\chi$, which is quantified with the mixing angle θ_{E_6} , through the equation provided below Table I.

TABLE I. Charge assignments for the fields in several models.

Model	\hat{Q}	\hat{U}^c	\hat{D}^c	\hat{L}	\hat{E}^c	\hat{H}_d	\hat{H}_u	\hat{S}
$2\sqrt{6} U(1)_\psi$	1	1	1	1	1	-2	-2	4
$2\sqrt{10} U(1)_\chi$	-1	-1	3	3	-1	-2	2	0

$$Q^i = Q_\chi^i \cos \theta_{E_6} + Q_\psi^i \sin \theta_{E_6}.$$

Moreover, v_s is now responsible for the spontaneous breaking of the $U(1)'$ symmetry, and hence the μ_{eff} term can be related to the breaking mechanism of a larger symmetry. The particle content of UMSSM is slightly richer than the MSSM. First of all, in addition to the S field, there should be also another gauge field associated with the $U(1)'$ group, which is denoted by Z' . Even though the current analyses provide strict bounds on Z' ($M_Z \geq 2.7\text{--}3.3$ TeV [18], $M_Z \geq 4.1$ TeV [18]), the signal processes in these analyses are based on the leptonic decay modes of Z' as $Z' \rightarrow \bar{l}l$, where l stands for the charged leptons of the first two families. However, as shown in a recent study [19], Z' may barely decay into two leptons; hence such strict bounds can be relaxed. Moreover, its neutral superpartner (\tilde{B}') is also included in the low energy spectrum as required by SUSY. It is interesting that there is no specific mass bound on \tilde{B}' , and it can be as light as $\mathcal{O}(100)$ GeV consistent with the current experimental constraints [20,21]. Since \tilde{B}' is allowed to mix with the other neutralinos, the LSP neutralino may reveal its manifestation through the $U(1)'$ sector in the collider and DM direct detection experiments.

Since the MSSM fields are nontrivially charged under the extra $U(1)'$ group, the model may not be anomaly free. To avoid possible anomalies, one may include exotic fields whose participation into the triangle vertices leads to anomaly cancellation. However, such fields usually yield heavy exotic mass eigenstates at the low scale. If one chooses a superpotential in which these exotic fields do not interact with the MSSM fields directly, their effects in the sparticle spectrum are quite suppressed by their masses. In this case, the model effectively reduces to UMSSM without the exotic fields. After all, the superpotential is

$$W = Y_u \hat{Q} \hat{H}_u \hat{U} + Y_d \hat{Q} \hat{H}_d \hat{D} + Y_e \hat{L} \hat{H}_d \hat{E} + h_s \hat{S} \hat{H}_d \hat{H}_u \quad (14)$$

and the corresponding SSB Lagrangian can be written as

$$-\mathcal{L}_{\text{UMSSM}}^{\text{SUSY}} = \mathcal{L}_{\text{MSSM}}^{\text{SUSY}} + m_S^2 |S|^2 + M_{\tilde{B}'} \tilde{B}' \tilde{B}' + (A_s h_s S H_u H_d + \text{H.c.}). \quad (15)$$

Employing Eqs. (14) and (15), the Higgs potential can be obtained as

$$V^{\text{tree}} = V_F^{\text{tree}} + V_D^{\text{tree}} + V_{\text{SUSY}}^{\text{tree}} \quad (16)$$

with

$$\begin{aligned} V_F^{\text{tree}} &= |h_s|^2 [|H_u H_d|^2 + |S|^2 (|H_u|^2 + |H_d|^2)] \\ V_D^{\text{tree}} &= \frac{g_1^2}{8} (|H_u|^2 + |H_d|^2)^2 + \frac{g_2^2}{2} (|H_u|^2 |H_d|^2 - |H_u H_d|^2) \\ &\quad + \frac{g^2}{2} (Q_{H_u} |H_u|^2 + Q_{H_d} |H_d|^2 + Q_S |S|^2) \\ V_{\text{SUSY}}^{\text{tree}} &= m_{H_u}^2 |H_u|^2 + m_{H_d}^2 |H_d|^2 + m_S^2 |S|^2 \\ &\quad + (A_s h_s S H_u H_d + \text{H.c.}), \end{aligned} \quad (17)$$

which yields the following tree-level mass for the lightest CP -even Higgs boson mass:

$$\begin{aligned} m_h^2 &= M_Z^2 \cos^2 2\beta \\ &\quad + (v_u^2 + v_d^2) \left[\frac{h_s^2 \sin^2 2\beta}{2} + g_{Y'}^2 (Q_{H_u} \cos^2 \beta + Q_{H_d} \sin^2 \beta) \right]. \end{aligned} \quad (18)$$

The second term in the square parentheses of Eq. (18) reflects the contribution from the $U(1)'$ sector, where $g_{Y'}$ is the gauge coupling associated with $U(1)'$, Q_{H_u} and Q_{H_d} are the charges of H_u and H_d under the $U(1)'$ group. After these contributions, the tree-level Higgs boson mass can be obtained as large as about 140 GeV for low $\tan \beta$, while it can be as heavy as about 115 GeV, when $\tan \beta$ is large [19]. Similarly, other Higgs bosons receive contributions from the $U(1)'$ sector, and the charged Higgs boson mass can be obtained at tree level as

$$m_{H^\pm}^2 = M_W^2 + \frac{\sqrt{2} h_s A_s v_s}{\sin(2\beta)} - \frac{1}{2} h_s^2 (v_d^2 + v_u^2). \quad (19)$$

In addition to the Higgs sector, the neutralino sector is also enlarged in UMSSM. Since it has a field whose VEV breaks $U(1)'$ symmetry, its fermionic superpartner mixes with the MSSM neutralinos, as in the NMSSM case. Moreover, since UMSSM possesses an extra $U(1)$ symmetry, the gaugino partner of the gauge field (Z') also mixes with the other neutralinos. In sum, there are six neutralinos in UMSSM, and their masses and mixing can be given in $(\tilde{B}', \tilde{B}, \tilde{W}, \tilde{h}_u, \tilde{h}_d, \tilde{S})$ basis as

$$\mathcal{M}_{\tilde{\chi}^0} = \left(\begin{array}{ccc|cc|c} M'_1 & 0 & 0 & g'_Y Q_{H_d} v_d & g'_Y Q_{H_u} v_u & g'_Y Q_S v_s \\ \hline 0 & & & & & 0 \\ 0 & & & & & 0 \\ g'_Y Q_{H_d} v_d & & \mathcal{M}_{\tilde{\chi}^0}^{\text{MSSM}}(\mu = \mu_{eff}) & & & -\frac{1}{\sqrt{2}} h_s v_u \\ g'_Y Q_{H_u} v_u & & & & & -\frac{1}{\sqrt{2}} h_s v_d \\ \hline g'_Y Q_S v_s & 0 & 0 & -\frac{1}{\sqrt{2}} h_s v_u & -\frac{1}{\sqrt{2}} h_s v_d & 0 \end{array} \right), \quad (20)$$

where M'_1 is the SSB mass of \tilde{B}' , and the first row and column code the mixing of \tilde{B}' with the other neutralinos. The middle part represents the MSSM neutralino masses and mixing, while the last column and row displays the mass and mixing for the MSSM singlet field as in the case of NMSSM. Similar to NMSSM, UMSSM does not propose any new charged particle; hence, the chargino sector remains the same as that in MSSM.

III. SCANNING PROCEDURE AND EXPERIMENTAL CONSTRAINTS

We have employed the SPHENO 3.3.3 package [22] obtained with SARAH 4.5.8 [23]. In this package, the weak scale values of the gauge and Yukawa couplings are evolved to the unification scale M_{GUT} via the renormalization group equations (RGEs). M_{GUT} is determined by the requirement of the gauge coupling unification, described as $g_1 = g_2$ for CMSSM and NMSSM, while it is as $g_1 = g_2 = g_{Y'}$ for UMSSM. Note that the UMSSM framework is not anomaly free, but its RGEs are being used, since the U(1)' models reduce to UMSSM effectively due to possible heavy exotic

states. This treatment can be improved with the inclusion of such exotic states in the RGEs. Even though g_3 does not appear in these conditions for M_{GUT} , it needs to take part in the gauge coupling unification condition. Concerning the contributions from the threshold corrections to the gauge couplings at the GUT scale arising from some unknown breaking mechanisms of the GUT gauge group, g_3 receives the largest contributions [24], and it is allowed to deviate from the unification up to about 3%. If a solution does not require this condition within this allowance, SPHENO does not generate an output for such solutions by default. Hence, the existence of an output file guarantees that the solutions are compatible with the unification condition, and g_3 deviates no more than 3%. With the boundary conditions given at M_{GUT} , all the SSB parameters along with the gauge and Yukawa couplings are evolved back to the weak scale. Note that each model yields different RGEs coded by SARAH in different model packages for SPHENO. We employ the packages called after the model names as MSSM, NMSSM and UMSSM. During our numerical investigation, we have performed random scans over the following parameter spaces of CMSSM, NMSSM and UMSSM:

CMSSM	NMSSM	UMSSM
$0 \leq m_0 \leq 5$ (TeV)	$0 \leq m_0 \leq 3$ (TeV)	$0 \leq m_0 \leq 3$ (TeV)
$0 \leq M_{1/2} \leq 5$ (TeV)	$0 \leq M_{1/2} \leq 3$ (TeV)	$0 \leq M_{1/2} \leq 3$ (TeV)
$1.2 \leq \tan \beta \leq 50$	$1.2 \leq \tan \beta \leq 50$	$1.2 \leq \tan \beta \leq 50$
$-3 \leq A_0/m_0 \leq 3$	$-3 \leq A_0/m_0 \leq 3$	$-3 \leq A_0/m_0 \leq 3$
$\mu > 0$	$0 \leq h_s \leq 0.7$	$0 \leq h_s \leq 0.7$
	$1 \leq v_s \leq 25$ (TeV)	$1 \leq v_s \leq 25$ (TeV)
	$-10 \leq A_s, A_\kappa \leq 10$ (TeV)	$-10 \leq A_s \leq 10$ (TeV)
	$0 \leq \kappa \leq 0.7$	$-\frac{\pi}{2} \leq \theta_{E_6} \leq \frac{\pi}{2}$

where m_0 is the universal spontaneous supersymmetry breaking (SSB) mass term for the matter scalars. This mass term is also set as $m_{H_u} = m_{H_d} = m_0$ in CMSSM, while m_{H_u} and m_{H_d} are calculated through the electroweak symmetry breaking (EWSB) conditions, which leads to $m_{H_u} \neq m_{H_d} \neq m_0$ in NMSSM and UMSSM. Similarly, $M_{1/2}$ is the universal SSB mass term for the gaugino fields, which includes one associated with the $U(1)'$ gauge group in UMSSM. $\tan\beta = \langle v_u \rangle / \langle v_d \rangle$ is the ratio of VEVs of the MSSM Higgs doublets, A_0 is the SSB term for the trilinear scalar interactions between the matter scalars and MSSM Higgs fields. Similarly, A_s is the SSB interaction between the S and $H_{u,d}$ fields, and A_κ is the SSB term for the triple self-interactions of the S fields. h_s and κ have defined before. Note that $\kappa = 0$ in the UMSSM case. Finally, v_s denotes the VEV of S fields. Recall that the μ term of MSSM is dynamically generated such that $\mu = h_s v_s / \sqrt{2}$. Its sign is assigned as a free parameter in MSSM, since the radiative electroweak symmetry breaking (REWSB) condition can determine its value but not sign. For simplicity, we forced it to be positive in NMSSM and in UMSSM by h_s and v_s . Finally, we set the top quark mass to its central value ($m_t = 173.3$ GeV) [25]. Note that the sparticle spectrum is not very sensitive in one or two sigma variation in the top quark mass [26], but it can shift the Higgs boson mass by 1–2 GeV [27].

The requirement of radiative electroweak symmetry breaking (REWSB) provides important theoretical constraints, since it excludes the solutions with $m_{H_u}^2 = m_{H_d}^2$ [9]. Besides, based on our previous experience from the numerical analyses over the parameter spaces of various SUSY models, REWSB requires $m_{H_u}^2$ to be more negative than $m_{H_d}^2$ at the low scale (see for instance [27]). In addition, the solutions are required to bring consistent values for the gauge and Yukawa couplings, gauge boson masses, top quark mass [28] etc. Such constraints are being imposed into SPHENO by default. In addition, the solutions must not yield color and/or charge breaking minima, which restricts the trilinear scalar interaction coupling in our scans as $|A_0| \leq 3m_0$, where m_0 is the universal mass term at the GUT scale for the SUSY scalars. Another important constraint comes from the relic abundance of the stable charged particles [29], which excludes the regions where charged SUSY particles such as stau and stop become the lightest supersymmetric particle (LSP). In our scans, we allow only the solutions for which one of the neutralinos is the LSP and the REWSB condition is satisfied.

In scanning the parameter space, we use our interface, which employs the Metropolis-Hasting algorithm described in [30]. After collecting the data, we impose the mass bounds on all the sparticles [31], and the constraint from the rare B decays such as $B_s \rightarrow \mu^+ \mu^-$ [6], $B_s \rightarrow X_s \gamma$ [32], and $B_u \rightarrow \tau \nu_\tau$ [33]. In addition, the WMAP bound [34] on the relic abundance of neutralino

LSP within 5σ uncertainty. Note that the current results from the Planck satellite [35] allow more or less a similar range for the DM relic abundance within 5σ uncertainty, when one takes the uncertainties in calculation. These experimental constraints can be summarized as follows:

$$\begin{aligned}
 m_h &= 123 - 127 \text{ GeV} \\
 m_{\tilde{g}} &\geq 1.8 \text{ TeV} \\
 M_{Z'} &\geq 2.5 \text{ TeV} \\
 0.8 \times 10^{-9} &\leq \text{BR}(B_s \rightarrow \mu^+ \mu^-) \leq 6.2 \times 10^{-9} (2\sigma) \\
 m_{\tilde{\chi}_1^0} &\geq 103.5 \text{ GeV} \\
 m_{\tilde{\tau}} &\geq 105 \text{ GeV} \\
 2.99 \times 10^{-4} &\leq \text{BR}(B \rightarrow X_s \gamma) \leq 3.87 \times 10^{-4} (2\sigma) \\
 0.15 &\leq \frac{\text{BR}(B_u \rightarrow \tau \nu_\tau)_{\text{MSSM}}}{\text{BR}(B_u \rightarrow \tau \nu_\tau)_{\text{SM}}} \leq 2.41 (3\sigma) \\
 0.0913 &\leq \Omega_{\text{CDM}} h^2 \leq 0.1363 (5\sigma). \tag{22}
 \end{aligned}$$

In addition to those listed above, we also employ the constraints on the SM-like Higgs boson decay processes obtained from the ATLAS [36] and CMS [37] analyses. We expect a strong impact from current bounds for $\text{BR}(B \rightarrow X_s \gamma)$ on the parameter space. Figure 1 displays the results for the impacts from the $B \rightarrow X_s \gamma$ and $h \rightarrow ZZ$ processes (where h denotes the SM-like Higgs boson) with plots in the $\text{BR}(B_s \rightarrow X_s \gamma) - m_{H^\pm}$ and $\text{BR}(h \rightarrow ZZ) - m_{H^\pm}$ planes for CMSSM. All points are compatible with the REWSB and neutralino LSP conditions. Green points satisfy the mass bounds and the constraints from the rare decays of the B meson. The blue points form a subset of green and they are consistent with the constraints from the SM-like Higgs boson decay processes. Note that the constraint from $\text{BR}(B_s \rightarrow X_s \gamma)$ is not applied in the left plane, but the bounds from these processes are represented with the horizontal solid lines. Similarly, the constraint from $\text{BR}(h \rightarrow ZZ)$ is not employed in the right plane, and the horizontal lines indicate the experimental bounds ($0.024 \leq \text{BR}(h \rightarrow ZZ) \leq 0.029$) within 2σ uncertainty [32,36,37]. As we expect, the constraint from the $\text{BR}(B_s \rightarrow X_s \gamma)$ process excludes a significant portion of the parameter space (green points below the bottom horizontal line); however, its impact barely affects the mass bound on the charged Higgs boson. We can find the $m_{H^\pm} \gtrsim 800$ GeV allowed by this constraints (see also [38]). On the other hand, the main impact on the parameter space (and hence on the charged Higgs boson mass) comes from those for the SM-like Higgs boson decays. The $\text{BR}(h \rightarrow ZZ) - m_{H^\pm}$ plane shows that the $h \rightarrow ZZ$ process excludes more than half of the parameter space (green and blue points below the bottom horizontal line in the right panel). According to the results in the $\text{BR}(h \rightarrow ZZ) - m_{H^\pm}$ plane, the solutions

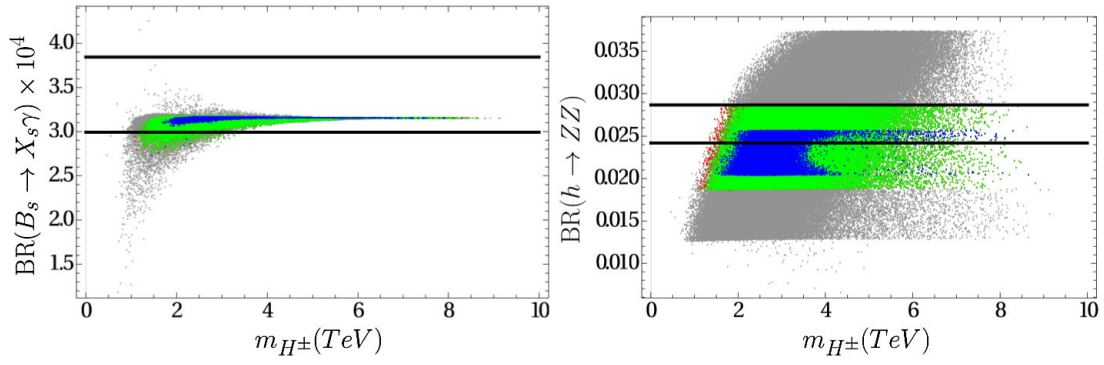


FIG. 1. CMSSM plots in the $\text{BR}(B_s \rightarrow X_s \gamma) - m_{H^\pm}$ and $\text{BR}(h \rightarrow ZZ) - m_{H^\pm}$ planes. All points are compatible with the REWSB and neutralino LSP conditions. Green points satisfy the mass bounds and the constraints from the rare decays of the B meson. The blue points form a subset of green and they are consistent with the constraints from the SM-like Higgs boson decay processes. Note that the constraint from $\text{BR}(B_s \rightarrow X_s \gamma)$ is not applied in the left plane, but the bounds from these processes are represented with the horizontal solid lines. Similarly, the constraint from $\text{BR}(h \rightarrow ZZ)$ is not employed in the right plane, and the horizontal lines indicate the experimental bounds from this process ($0.024 \leq \text{BR}(h \rightarrow ZZ) \leq 0.029$) within 2σ uncertainty [32,36,37].

with $m_{H^\pm} \lesssim 2$ TeV are excluded by the $h \rightarrow ZZ$ process. Note that the universal boundary conditions of CMSSM restrict results more, and if nonuniversality is employed, the lower mass for the charged Higgs boson can be found at about 1 TeV consistently with the current constraints including that from the $h \rightarrow ZZ$ process [39]. Thus, our results will also mean that some possible signal channels require to impose nonuniversal boundary conditions in the MSSM framework to be available.

On the other hand, one can investigate the impacts of these constraints on the fundamental parameter space of NMSSM and UMSSM as shown in Fig. 2 with plots for the impacts of $\text{BR}(B_s \rightarrow X_s \gamma)$ (left) and $\text{BR}(h \rightarrow ZZ)$ (right) on the parameter space of NMSSM (top) and UMSSM (bottom). The color coding is the same as Fig. 1. The results in Fig. 2 shows that the constraint from $h \rightarrow ZZ$ has a strong impact in both models. However, even though this constraint excludes more than half of the solutions, it does

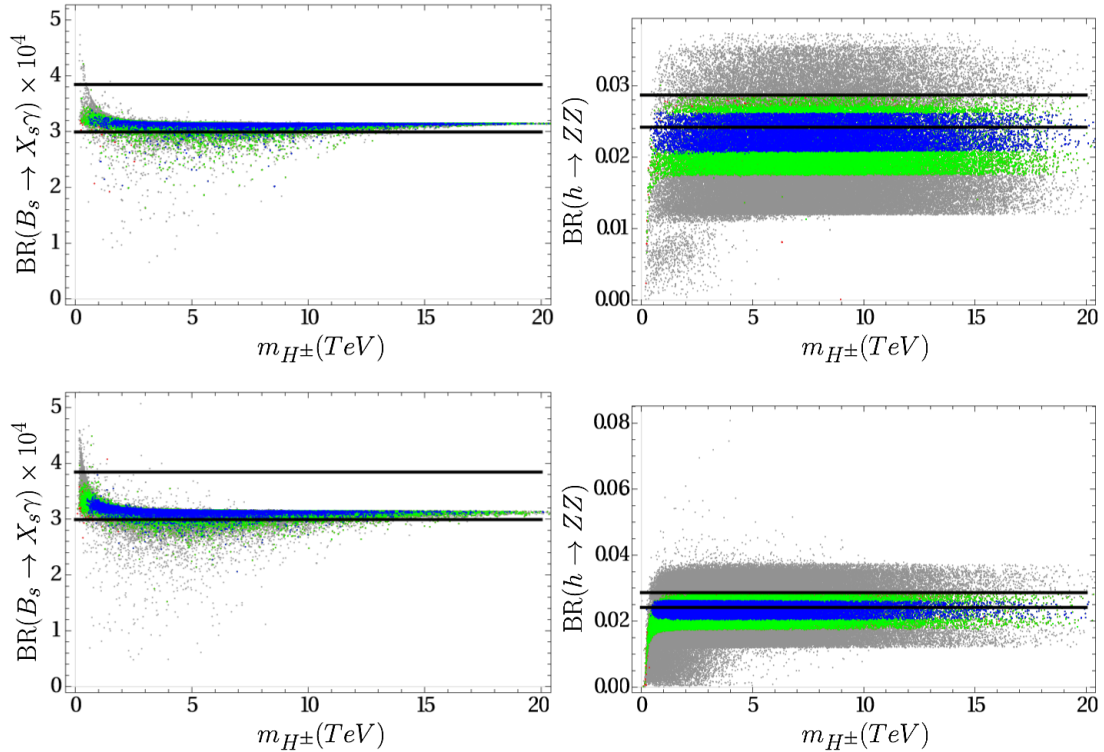


FIG. 2. Plots for the impacts of $\text{BR}(B_s \rightarrow X_s \gamma)$ (left) and $\text{BR}(h \rightarrow ZZ)$ (right) on the parameter space of NMSSM (top) and UMSSM (bottom). The color coding is the same as Fig. 1.

not bound the charged Higgs mass from below, in contrast to CMSSM. Note that lighter mass scales for the charged Higgs boson can be allowed, if one employs relatively milder bounds from the $h \rightarrow ZZ$ process.

We have emphasized the bounds on the Higgs boson [40] and the gluino [41], since they have drastically changed since the Linear electron-positron (LEP) collider era. We have employed the two-loop RGEs in calculation of the Higgs boson mass. The uncertainty in the Higgs boson mass calculation arises mostly from the uncertainties in values of the strong gauge coupling and top quark masses, which yield about 3 GeV deviation in the Higgs boson mass calculation [42]. In addition, the large SUSY scale (M_{SUSY}) worsens the uncertainty in the Higgs boson mass calculation [43]. Note that there are more precise calculations available to improve the results for the Higgs boson mass (see for instance [44]). In addition, we have employed the LEP II mass bounds on the lightest chargino and stau. Although the mass bounds have recently been updated on these particles [45,46], these bounds are model dependent and based on specific decay channels of the chargino. While we employ the LEP II bounds on our plots, their masses will be discussed briefly later. In addition, the current mass bounds on Z' are established as $M_{Z'} \gtrsim 4.1$ TeV [18]. On the other hand, this bound can vary model dependently, and a most recent study [47] has shown that $M_{Z'} \gtrsim 2.5$ TeV can survive, if Z' is leptophobic. Based on our previous study [19], which was conducted in the similar parameter space, the leptonic decay processes of Z' are found as $\text{BR}(Z' \rightarrow ll) \lesssim 14\%$. Since the leptonic decays of Z' are found rather low, we set the mass bound on Z' as $M_{Z'} \geq 2.5$ TeV. The mass bound on Z' depends on the gauge coupling associated with the $U(1)'$ group which varies with θ_{E_6} . Thus, some of the solutions represented in our study can be excluded by the experimental analyses [18].

When the LSP is required to be one of the neutralinos, the DM relic abundance constraint will be highly effective to shape the fundamental parameter space, since the relic abundance of LSP neutralino is usually realized greater than the current measurement over most of the fundamental parameter space. Once one can identify the regions compatible with the current WMAP and Planck results, they can be analyzed further against the results from the direct detection [48], indirect detection [49] and collider experiments [50]. However, all these detailed analyses are out of the scope of our study. We apply only the relic abundance constraint on the LSP neutralino to show that the regions of interest for the charged Higgs boson phenomenology can also be compatible with the relic abundance bound from the current measurements, and they can be also tested under the light of the DM constraints in possible future studies. In this context, the DM implications obtained within our analyses can be improved with more thorough analyses devoted to DM. The DM observables in our scan are calculated by MICROMEAS [51] obtained by SARAH [23].

We will apply the constraints mentioned in this section subsequently, and thus, before concluding this section, it might be necessary to mention the color convention which we will use in the next sections in presenting the results. The following is the list that summarizes what color satisfies which constraints:

Grey: REWSB and neutralino LSP conditions.

Red: REWSB, neutralino LSP and Higgs boson mass constraint.

Green: REWSB, neutralino LSP, Higgs boson mass constraint, SUSY particle mass bounds, and B-physics constraints.

Blue: REWSB, neutralino LSP, Higgs boson mass constraint, SUSY particle mass bounds, B-physics constraints, LHC constraints on the Higgs boson couplings.

Black: REWSB, neutralino LSP, Higgs boson mass constraint, SUSY particle mass bounds, B-physics constraints, LHC constraints on the Higgs boson couplings, and WMAP and Planck constraints on the relic abundance of neutralino LSP within 5σ .

From black to grey, each color is always on top of the previous one in the order as listed above in a way that the black always stays on top of all other colors in the plots.

IV. FUNDAMENTAL PARAMETER SPACE AND MASS SPECTRUM

In this section, we consider the fundamental parameter space, shaped by the experimental constraints discussed in the previous section, and discuss the charged Higgs mass along with the mass spectrum for other particles, which might be relevant to decay modes of the charged Higgs boson. Figure 3 displays our results with plots in the $m_0 - m_{H^\pm}$ and $M_{1/2} - m_{H^\pm}$ planes for CMSSM (left panel), NMSSM (middle panel) and UMSSM (right panel). All points are consistent with the REWSB and neutralino LSP. Our color convention is as listed at the end of Sec. III. In the CMSSM case, as seen from the left panel, the charged Higgs can be as heavy as about 8 TeV in the range of the fundamental parameters given in Eq. (21).

These results in CMSSM arise from the fact that CMSSM yields mostly bino-like LSP neutralino $\mu \gg M_2 \sim 2M_1$ [52], where μ is the Higgsino mass parameter, while M_2 and M_1 are the SSB masses of Wino and Bino, respectively. The problem with bino-like DM is that its relic abundance is usually much larger than the current measurements of the WMAP [34] and Planck [35] satellites, and one needs to identify some coannihilation channels which take part in reducing the LSP neutralino's relic abundance down to the current ranges [53]. However, the void direct signals for supersymmetry from the LHC experiments yield quite heavy spectrum in the low scale implications of CMSSM, and the mass scales are usually out of the possible coannihilation scenarios. On the other hand, even if the neutralino sector is extended only a single

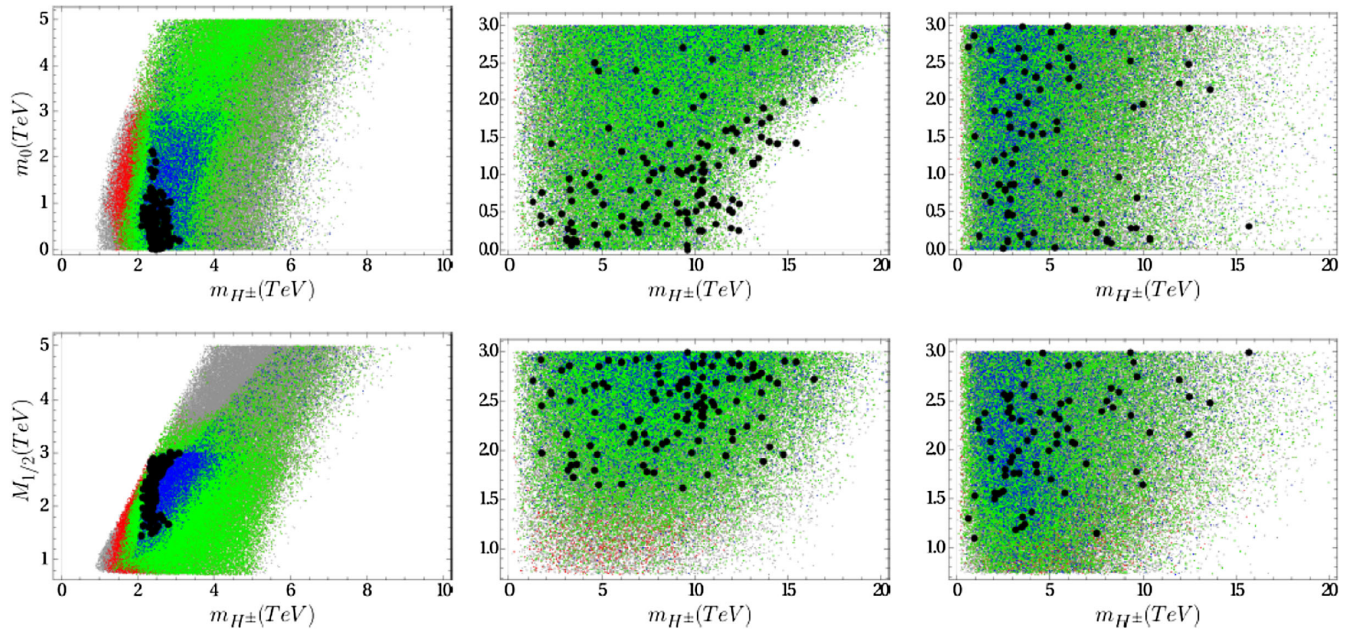


FIG. 3. Plots in the $m_0 - m_{H^\pm}$ and $M_{1/2} - m_{H^\pm}$ planes for CMSSM (left panel), NMSSM (middle panel) and UMSSM (right panel). All points are consistent with the REWSB and neutralino LSP. Our color convention is as listed at the end of Sec. III.

flavor, the region of the parameter space allowed by the DM observations becomes quite wide open [21], as a result of mixing the extra flavor state with the MSSM neutralinos. However, as seen from the bottom left panel of Fig. 3, the charged Higgs boson cannot be lighter than about 1.5 TeV when one employs the LHC constraints (green). Even though we do not find solutions for $m_{H^\pm} \lesssim 2$ TeV after applying all the constraints listed in Sec. III, some recent studies [54] have shown that $m_{H^\pm} \gtrsim 1.5$ TeV can be consistent with the DM constraints. Such a lower bound on the charged Higgs boson mass mostly arises from the rare B-meson decay process, $B_s \rightarrow X_s \gamma$, where X_s is a suitable bound state of the strange quark. The strong agreement between the experimental measurements ($\text{BR}^{\text{exp}}(B_s \rightarrow X_s \gamma) = (3.43 \pm 0.22) \times 10^{-4}$ [32]) and the Standard Model prediction ($\text{BR}^{\text{SM}}(B_s \rightarrow X_s \gamma) = (3.15 \pm 0.23) \times 10^{-4}$ [55]) strongly enforces a lower bound on the charged Higgs boson mass. However; as have been shown before, these constraints from the rare B-meson decays restrict the charged Higgs boson mass as $m_{H^\pm} \gtrsim 800$ GeV. The strongest restriction comes from the $h \rightarrow ZZ$ process, which excludes the solutions with $m_{H^\pm} \lesssim 2$ TeV (blue points). In contrast to the results in CMSSM, the mass range of the charged Higgs boson is quite wide in NMSSM and UMSSM, as is seen from the middle and right panels respectively, and the solutions can yield m_{H^\pm} from about 1 to 15 TeV, after the experimental constraints are employed. This wide mass range partly arises from the nonuniversality in m_{H_d} and m_{H_u} in NMSSM and UMSSM. In addition, such a wide region allowed by the DM observations reflects the significant effect of extending the neutralino sector of MSSM even with one extra flavor

state. The recent studies have shown that new flavor states, which are allowed to mix with the MSSM neutralinos, can significantly alter the DM implications [21]. The fundamental parameter space for NMSSM and UMSSM is restricted based on our previous studies [19,56], which explored the regions with acceptable fine-tuning in the fundamental parameter space of UMSSM.

The other fundamental parameters are A_0 and $\tan \beta$, and the results in terms of these parameters are represented in Fig. 4 with plots in the $\tan \beta - m_{H^\pm}$ and $A_0/m_0 - m_{H^\pm}$ planes for CMSSM (left panel), NMSSM (middle panel) and UMSSM (right panel). The color coding is the same as Fig. 3. As seen from the top panels, $\tan \beta$ is a strong parameter in m_{H^\pm} , and one can realize the heavy charged Higgs boson only when $\tan \beta \lesssim 10$ in the CMSSM and NMSSM frames, while it is restricted to moderate values as $20 \lesssim \tan \beta \lesssim 30$ in UMSSM. On the other hand, there is no specific restriction in A_0 , and as seen from the bottom panels, it is possible to realize the whole allowed range of m_{H^\pm} for any A_0 .

After presenting the fundamental parameter space of the models, we consider the mass spectrum, which reveals which particles the charged Higgs boson may kinematically be allowed to decay. First we present the stop and sbottom masses in Fig. 5 with plots in the $m_{\tilde{t}_1} - m_{H^\pm}$ and $m_{\tilde{b}_1} - m_{H^\pm}$ planes for CMSSM (left panel), NMSSM (middle panel) and UMSSM (right panel). If the solutions with $m_{H^\pm} \gtrsim m_{\tilde{t}} + m_{\tilde{b}}$ can be realized, then the charged Higgs boson can participate in the processes $H^\pm \rightarrow \tilde{t} \tilde{b}$. As seen from the middle and right panels, if the charged Higgs boson is allowed to be heavy enough, there is a possibility for the decay process $H^\pm \rightarrow \tilde{t} \tilde{b}$. However, since the

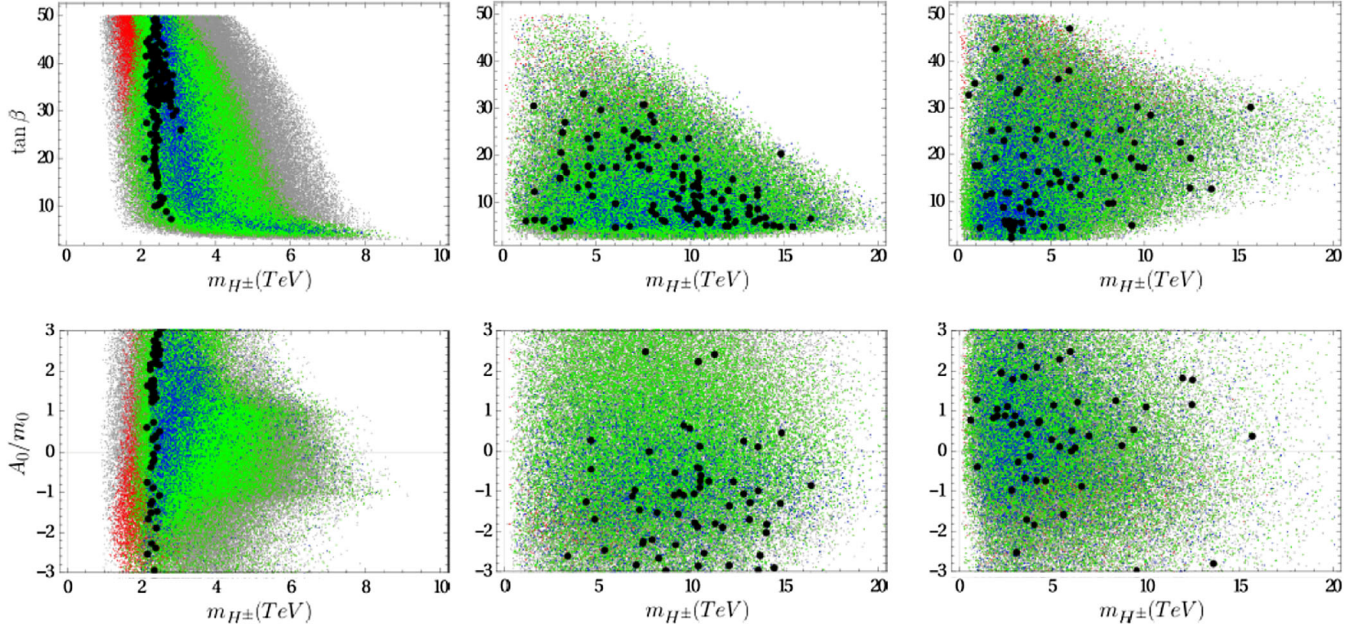


FIG. 4. Plots in the $\tan\beta - m_{H^\pm}$ and $A_0/m_0 - m_{H^\pm}$ planes for CMSSM (left panel), NMSSM (middle panel) and UMSSM (right panel). The color coding is the same as Fig. 3.

relevant background generated by the decay processes involving with the top quark significantly suppresses the possible signals from stop [57], such decays of the charged Higgs boson may not provide a detectable track.

Figure 6 displays our results with another pair of supersymmetric particles, stau and sneutrino, which the charged Higgs boson can decay, with plots in the $m_{\tilde{\tau}_1} - m_{H^\pm}$ and $m_{\tilde{\nu}} - m_{H^\pm}$ planes for CMSSM (left panel),

NMSSM (middle panel) and UMSSM (right panel). The color coding is the same as Fig. 3. The current bound on a charged slepton can be expressed as $m_{\tilde{\tau}} \gtrsim 400$ GeV [58]. Such bounds rely on the chargino-neutralino production, which differs from model to model; thus it can vary depending on the mass spectrum. Considering the model dependence of such bounds, even if we employed the LEP2 bounds, the LHC and DM constraints bound the stau mass

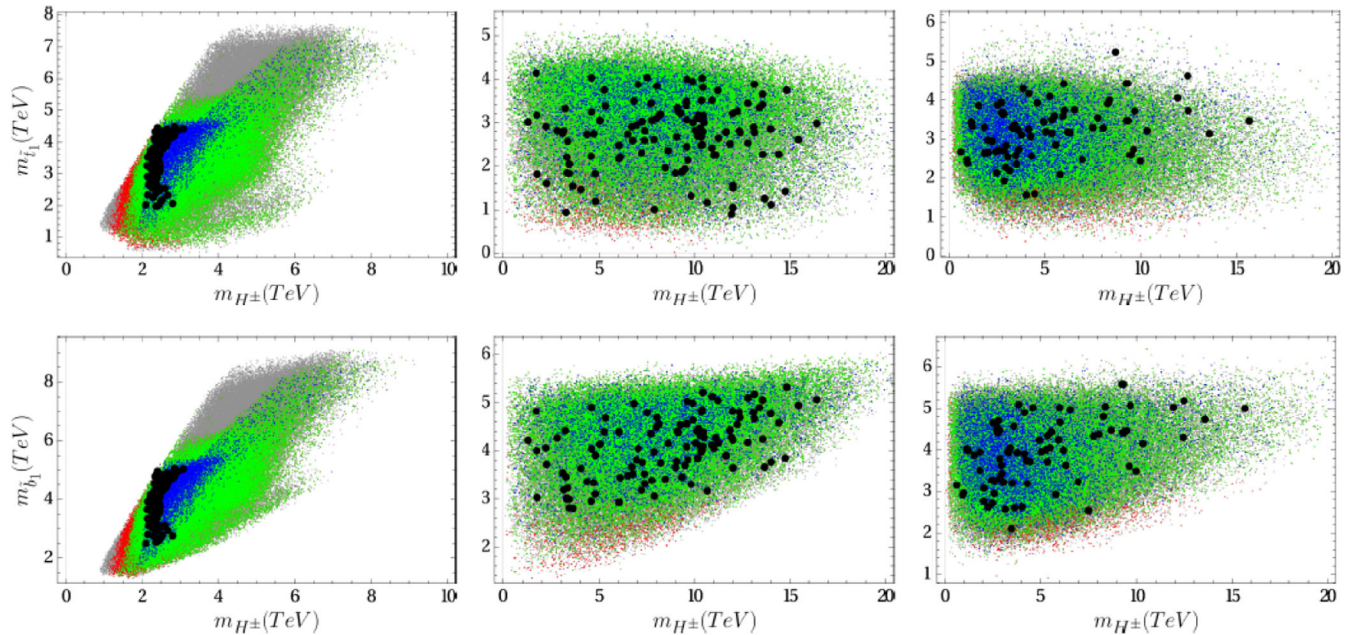


FIG. 5. Plots in the $m_{\tilde{\tau}_1} - m_{H^\pm}$ and $m_{\tilde{\nu}} - m_{H^\pm}$ planes for CMSSM (left panel), NMSSM (middle panel) and UMSSM (right panel). The color coding is the same as Fig. 3.

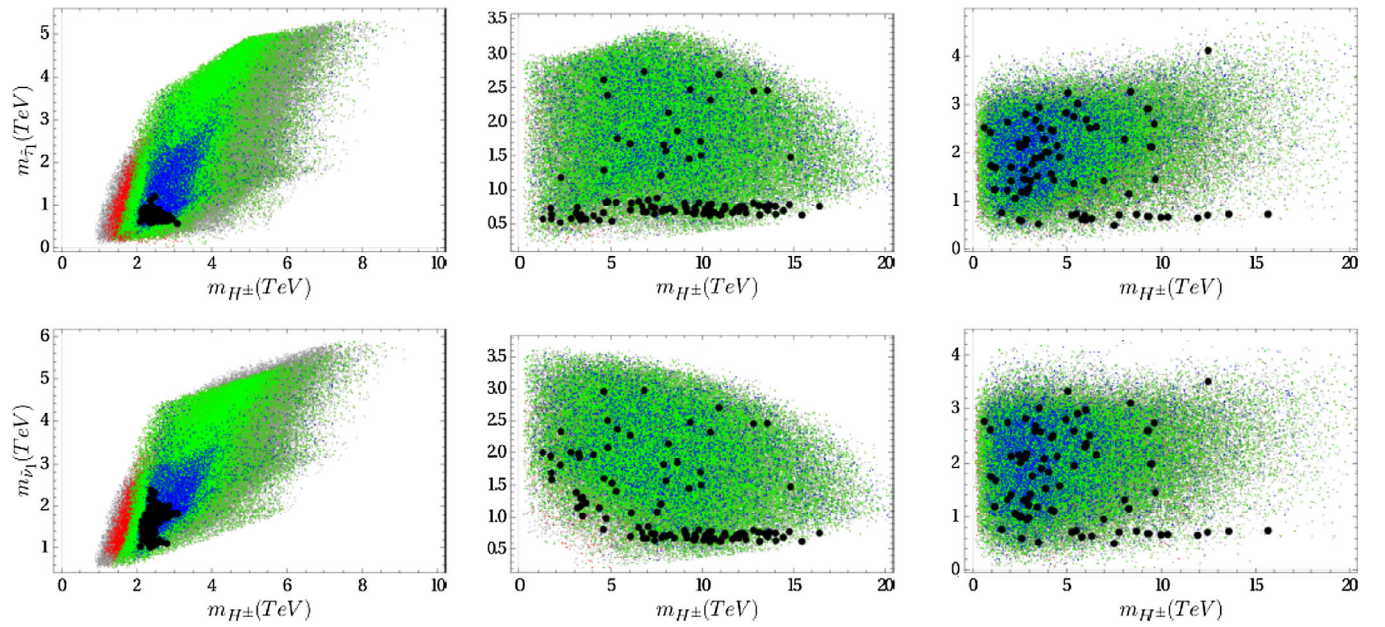


FIG. 6. Plots in the $m_{\tilde{\tau}_1} - m_{H^\pm}$ and $m_{\tilde{\nu}} - m_{H^\pm}$ planes for CMSSM (left panel), NMSSM (middle panel) and UMSSM (right panel). The color coding is the same as Fig. 3.

from below as $m_{\tilde{\tau}} \gtrsim 500$ GeV in all CMSSM, NMSSM and UMSSM as seen from the top panels. Similarly the sneutrino mass is also bounded as $m_{\tilde{\nu}} \gtrsim 1$ TeV.

Figure 7 shows the neutralino masses and the charged Higgs boson mass with plots in the $m_{\tilde{\chi}_1^0} - m_{H^\pm}$ and $m_{\tilde{\chi}_i^0} - m_{H^\pm}$ planes for CMSSM (left panel), NMSSM (middle panel) and UMSSM (right panel), where i stands for the number identifying the heaviest neutralino in models as

$i = 4$ for CMSSM, $i = 5$ for NMSSM, and $i = 6$ for UMSSM. The color coding is the same as Fig. 3. All models allow the LSP neutralino to be only as heavy as about 1.5 TeV. The upper bound on the neutralino LSP mass arises from the range assigned to $M_{1/2}$ in scanning the fundamental parameter spaces of the models. The lower bound, on the other hand, arises mostly from the heavy bound on the gluino mass, while the other constraints may

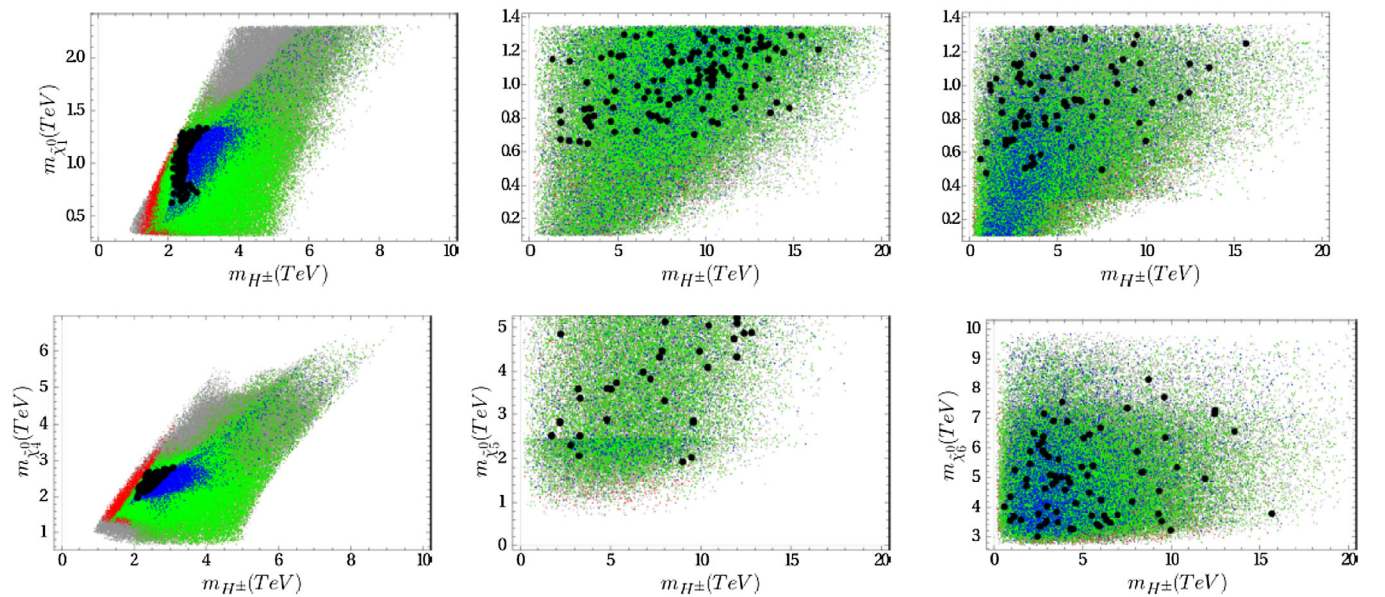


FIG. 7. Plots in the $m_{\tilde{\chi}_1^0} - m_{H^\pm}$ and $m_{\tilde{\chi}_i^0} - m_{H^\pm}$ planes for CMSSM (left panel), NMSSM (middle panel) and UMSSM (right panel), where i stands for the number identifying the heaviest neutralino in models as $i = 4$ for CMSSM, $i = 5$ for NMSSM, and $i = 6$ for UMSSM. The color coding is the same as Fig. 3.

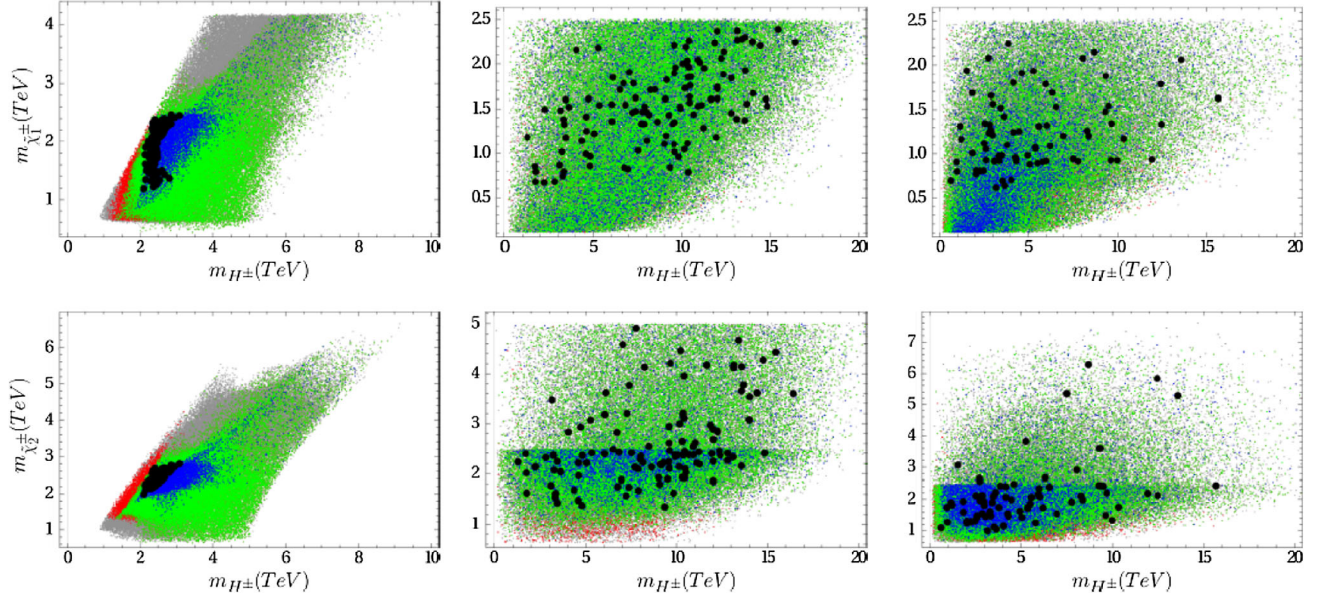


FIG. 8. Plots in the $m_{\tilde{\chi}_1^\pm} - m_{H^\pm}$ and $m_{\tilde{\chi}_2^\pm} - m_{H^\pm}$ planes for CMSSM (left panel), NMSSM (middle panel) and UMSSM (right panel). The color coding is the same as Fig. 3.

also have minor effects. Without the relic density constraint, the neutralino LSP mass can be as low as about 400 GeV in CMSSM, while the lower bound can be as low as about 100 GeV in NMSSM and UMSSM (blue). However, the WMAP and Planck bounds on the relic abundance of neutralino LSP can be satisfied when $m_{\tilde{\chi}_1^0} \gtrsim 500$ GeV in all models. The heaviest neutralino $\tilde{\chi}_i^0$ in CMSSM ($i = 4$) cannot be lighter than about 2 TeV, while its mass is bounded from above as $m_{\tilde{\chi}_4^0} \lesssim 3$ TeV. While NMSSM and UMSSM reveal a similar bound from below at about 500 GeV, the heaviest neutralino mass in these models can be realized in multi-TeV scale as $m_{\tilde{\chi}_5^0} \lesssim 5$ TeV in NMSSM and $m_{\tilde{\chi}_5^0} \lesssim 10$ TeV in UMSSM.

Since the decay modes of H^\pm including a neutralino happen along with also a chargino, we conclude this section by considering the chargino masses in the models as shown in Fig. 8 with plots in the $m_{\tilde{\chi}_1^\pm} - m_{H^\pm}$ and $m_{\tilde{\chi}_2^\pm} - m_{H^\pm}$ planes for CMSSM (left panel), NMSSM (middle panel) and UMSSM (right panel). The color coding is the same as Fig. 3. The solutions in the CMSSM framework are allowed by the constraints only when they yield $m_{\tilde{\chi}_1^\pm} \gtrsim 1$ TeV (seen from the black points). Even though it is kinematically allowed ($m_{H^\pm} \sim m_{\tilde{\chi}_1^0} + m_{\tilde{\chi}_1^\pm}$), CMSSM may not provide significant decay processes in which the charged Higgs boson decays into a chargino and neutralino. On the other hand, the same constraints can allow lighter chargino solutions in NMSSM and UMSSM as $m_{\tilde{\chi}_1^\pm} \gtrsim 500$ GeV, while the heavier mass scales for the charged Higgs boson ($\gtrsim 10$ TeV) are also allowed. In this context, NMSSM and UMSSM may distinguish themselves from CMSSM, if they can yield significant $H^\pm \rightarrow \tilde{\chi}^0 \tilde{\chi}^\pm$ processes. The bottom

panels show also the second chargino may be effective in the charged Higgs decay modes, since the heavier charged Higgs boson is allowed and the constraints bound the second chargino mass from below as $m_{\tilde{\chi}_2^\pm} \gtrsim 2$ TeV in CMSSM.

V. PRODUCTION AND DECAY MODES OF H^\pm

Direct production processes of the charged Higgs boson at the LHC are rather difficult, since its production rate is proportional to the Yukawa couplings of the Higgs bosons with the quarks from the first two families. It is rather suppressed even when the charged Higgs boson is light, because the Yukawa couplings associated with the first two-family matter fields are quite small. On the other hand, the charged Higgs bosons can be produced through the top-pair productions if they are sufficiently light that the $t \rightarrow H^\pm b$ process is kinematically allowed. In such processes, the charged Higgs boson can leave its marks through the $H^\pm \rightarrow \tau^\pm b$ decay processes. In the cases with heavy charged Higgs bosons, the charged Higgs boson is produced at the LHC in association with either top quark [59] or W^\pm boson [60]. The production processes associated with top quark do not provide a clear signal due to a large number of jets involved in the final states. Nevertheless, those with the W^\pm boson might be expected to be a relatively clear signal, but such processes are suppressed by the irreducible background processes from the top-pair production processes [61]. In this context, it is not easy to detect the charged Higgs boson at the LHC. Even though an exclusion limit is provided for the charged Higgs boson, it can be excluded up to $m_{H^\pm} \sim 600$ GeV only for low $\tan\beta$ (~ 1) [59], which allows lighter charged Higgs boson solutions when $\tan\beta$ is large.

Before considering the possible decay modes, we present the possible production channels for the charged Higgs production over some benchmark points in Table II. These values were obtained after implementing our models into CALCHEP [62]. The points have been chosen so as to be consistent with the employed constraints discussed in Sec. III. The largest contributions to the charged Higgs production come from the processes involving with the top quark with the cross section $\sim 10^{-5}$ pb in CMSSM, while these processes can reach up to $\sigma \sim 10^{-3}$ pb in NMSSM and $\sigma \sim 10^{-2}$ pb in UMSSM. Even though the improvement in the latter models is quite significant, it is mostly because of the different mass scales of the charged Higgs boson. As discussed in the previous section, $m_{H^\pm} \gtrsim 2$ TeV is not allowed by the constraints in CMSSM, $m_{H^\pm} \gtrsim 1$ TeV in NMSSM and $m_{H^\pm} \gtrsim 500$ GeV in UMSSM are allowed. However, considering $\sigma(pp \rightarrow tH^\pm)$, one should still note that NMSSM still yields one magnitude larger cross section ($\sim 10^{-4}$ pb) in comparison to CMSSM and UMSSM for this production channel, if one considers the similar mass scales for the charged Higgs boson ($m_{H^\pm} \sim 2$ TeV). A similar discussion holds for $\sigma(pp \rightarrow t\bar{b}H^\pm)$. The other channels can also be seen in Table II, and as stated before, they are either negligible or a few magnitudes smaller than those involving with top quark.

Despite such small cross sections in comparison to, for instance, the SM-like Higgs boson [63], some possible signal processes relevant to the charged Higgs boson

become observable with a larger center of mass and luminosity. In addition, as stated before, the charged Higgs decays are crucial, since it does not exist in the SM, and these decays can also be distinguishing between models. In this sense, we consider its decays and discuss the channels in a variety of SUSY models, which may play an important role in detecting the charged Higgs boson in future collider experiments. Depending on its mass, the charged Higgs boson can decay into either a pair of SUSY particles or the SM particles. Since the current LHC results imply rather a heavy mass spectrum for the squarks and gluinos, it might be possible to realize $H^\pm \rightarrow \tilde{t}\tilde{b}(\tilde{\nu}_\tau)$ processes which yield matter sparticles in their final states. However, these channels are hardly possible when the SUSY models are constrained from the GUT scale with the universal boundary conditions. However, it might still be possible that the charged Higgs boson can decay into a pair of chargino-neutralino. If SUSY particles are so heavy that the charged Higgs is not kinematically allowed to decay into the SUSY particles, then the SM particles take over and provide dominant decay channels. Since only the Yukawa couplings to the third family are significant, the final states are expected to include either third family quarks or leptons. The dominant decay channel is realized as $H^\pm \rightarrow tb$. Indeed, it is not surprising to realize the dominant channel as $H^\pm \rightarrow tb$ in all the cases when the charged Higgs boson is heavy, while other decay channels can also be identified up to considerable percentage in some models. In this context, we start presenting our results

TABLE II. The charged Higgs boson production modes and cross sections over some benchmark points (we used the center of mass energy $\sqrt{s} = 14$ TeV). The points have been chosen so as to be consistent with all of the employed constraints discussed in Sec. III.

Observables	CMSSM		NMSSM		UMSSM	
	m_{H^\pm} (GeV)	σ (pb)	m_{H^\pm} (GeV)	σ (pb)	m_{H^\pm} (GeV)	σ (pb)
$pp \rightarrow tH^\pm$	2019	4.5×10^{-5}	1011	1.0×10^{-3}	551	1.6×10^{-2}
	3001	3.1×10^{-6}	2055	1.2×10^{-4}	1015	8.3×10^{-4}
	4002	1.0×10^{-7}	5849	5.8×10^{-9}	2061	1.7×10^{-5}
$pp \rightarrow W^\mp H^\pm$	2019	5.2×10^{-6}	1011	1.3×10^{-4}	551	1.0×10^{-3}
	3001	4.2×10^{-7}	2055	1.8×10^{-5}	1015	6.4×10^{-5}
	4002	1.7×10^{-8}	5849	1.3×10^{-9}	2061	2.0×10^{-6}
$pp \rightarrow H^\mp H^\pm$	2019	4.8×10^{-8}	1011	4.0×10^{-4}	551	2.7×10^{-4}
	3001	3.7×10^{-10}	2055	5.9×10^{-6}	1015	1.0×10^{-5}
	4002	1.5×10^{-12}	5849	3.0×10^{-18}	2061	4.0×10^{-8}
$pp \rightarrow H_{1,2,3}^0 H^\pm$	2019	1.6×10^{-8}	1011	5.2×10^{-6}	551	1.3×10^{-4}
	3001	9.3×10^{-11}	2055	1.5×10^{-8}	1015	4.4×10^{-6}
	4002	2.4×10^{-13}	5849	1.8×10^{-15}	2061	1.3×10^{-8}
$pp \rightarrow t\bar{b}H^\pm$	2019	1.7×10^{-5}	1011	4.1×10^{-2}	551	7.2×10^{-3}
	3001	1.4×10^{-6}	2055	1.8×10^{-2}	1015	3.4×10^{-4}
	4002	3.2×10^{-8}	5849	1.7×10^{-9}	2061	6.7×10^{-7}

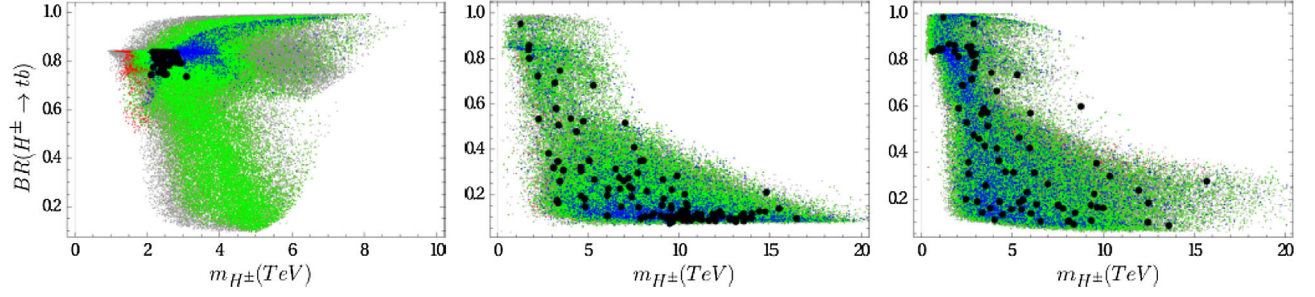


FIG. 9. The plots in the $BR(H^\pm \rightarrow tb) - m_{H^\pm}$ plane for CMSSM (left), NMSSM (middle) and UMSSM (right). The color coding is the same as Fig. 3.

for the $H^\pm \rightarrow tb$ process first, then we include other possible channels in our consideration.

A. $H^\pm \rightarrow tb$

Figure 9 represents our results for $BR(H^\pm \rightarrow tb)$ in correlation with m_{H^\pm} in CMSSM (left), NMSSM (middle) and UMSSM (right). As mentioned before, it provides the main decay channel for the charged Higgs boson in a possible signal, which could be detected in future collider experiments. When the DM constraints are applied (black points) top of the LHC constraints, CMSSM allows this channel only up to 80%, and it leaves a slight open window for the other possible decay modes. The constraints also bound this process from below as $BR(H^\pm \rightarrow tb) \gtrsim 70\%$. Hence, even though CMSSM allows some other channels, their branching ratios cannot be larger than 30%. In the case of NMSSM, it is possible to find solutions in which the charged Higgs boson only decays into tb , there is not any lower bound provided by the constraints. In other words, it is possible to realize $BR(H^\pm \rightarrow tb) \sim 10\%$, which means one can identify some other channels as the main channel, which are discussed later. Similar results can be found also in the UMSSM framework. In this context, there is a wide portion in the fundamental parameter space of NMSSM and UMSSM which distinguishes these models from CMSSM.

B. $H^\pm \rightarrow \tau\nu$

Figure 10 displays our result for the $BR(H^\pm \rightarrow \tau\nu)$ in correlation with m_{H^\pm} in CMSSM (left), NMSSM (middle)

and UMSSM (right). The color coding is the same as Fig. 3. All three models allow this channel only up to about 20%. This channel is expected to be dominant when $H^\pm \rightarrow tb$ is not allowed, i.e., $m_{H^\pm} < m_t + m_b$ [64]. Even though there is not a certain constraint through this leptonic decay of the charged Higgs, and it can provide a relatively clearer signal and less uncertainty, it may not display a possible signal and distinguish the models through these leptonic processes.

C. $H^\pm \rightarrow \tilde{\chi}_i^\pm \tilde{\chi}_j^0$

Figure 11 shows the results for the $BR(H^\pm \rightarrow \tilde{\chi}_1^0 \tilde{\chi}_1^\pm)$ in correlation with m_{H^\pm} in CMSSM (left), NMSSM (middle) and UMSSM (right). The color coding is the same as Fig. 3. Even though it is possible to realize this process up to about 8% (green) in CMSSM, the LHC measurements for the SM-like Higgs boson (blue) bound it as $BR(H^\pm \rightarrow \tilde{\chi}_1^0 \tilde{\chi}_1^\pm) \gtrsim 2\%$. However, these solutions do not satisfy the WMAP and Planck bounds on the relic abundance of the LSP neutralino. When one employs the DM constraints (black) it is seen that $BR(H^\pm \rightarrow \tilde{\chi}_1^0 \tilde{\chi}_1^\pm) \lesssim 1\%$. Hence, a possible signal involving with the $H^\pm \tilde{\chi}_1^0 \tilde{\chi}_1^\pm$ process is hardly realized in the CMSSM framework, while it is open in the NMSSM and UMSSM frameworks up to about 20%–25% consistently with all the constraints including the DM ones. Note that even though the solutions presented in Fig. 11 are enough to claim a sensible difference from CMSSM, better results for the branching ratios in NMSSM and UMSSM may still be obtained with more thorough statistics.

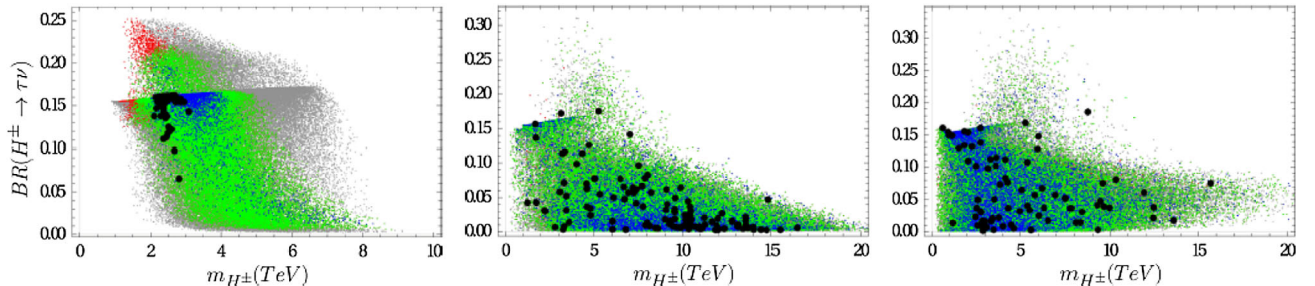


FIG. 10. The plots in the $BR(H^\pm \rightarrow \tau\nu) - m_{H^\pm}$ plane for CMSSM (left), NMSSM (middle) and UMSSM (right). The color coding is the same as Fig. 3.

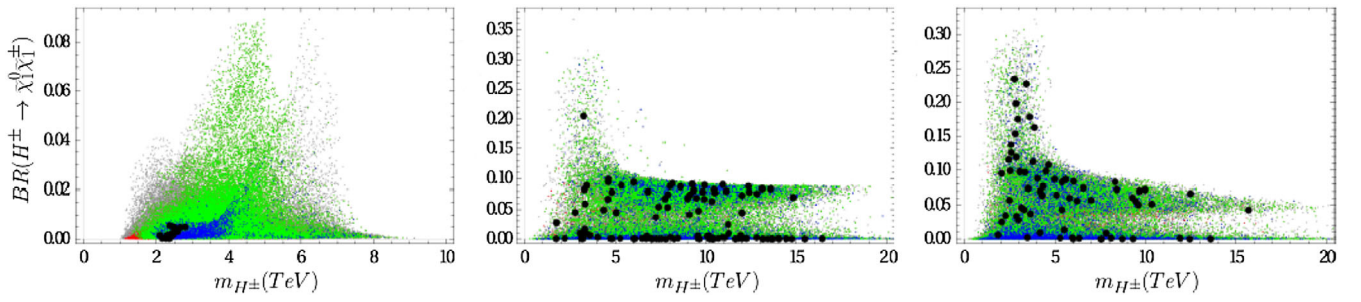


FIG. 11. The plots in the $\text{BR}(H^\pm \rightarrow \tilde{\chi}_1^0 \tilde{\chi}_1^\pm) - m_{H^\pm}$ plane for CMSSM (left), NMSSM (middle) and UMSSM (right). The color coding is the same as Fig. 3.

As discussed in Sec. IV, the heavier neutralino and chargino mass eigenstates are allowed to participate in $H^\pm \rightarrow \tilde{\chi}_i^0 \tilde{\chi}_j^\pm$. However, the heavier ones continue to decay into the lighter mass eigenstates, and each decay cascade gives a suppression unless their branching ratio is large ($\text{BR} \sim 100\%$). In this context, even though their signal is not as strong as $H^\pm \rightarrow \tilde{\chi}_1^0 \tilde{\chi}_1^\pm$, their contributions would be at the order of minor contributions in comparison to $\text{BR}(H^\pm \rightarrow \tilde{\chi}_1^0 \tilde{\chi}_1^\pm)$.

In addition to the charginos and neutralinos, the Higgs boson can be allowed to decay into some other supersymmetric particles, which could be, in principle, a pair of $\tilde{t}\tilde{b}$ or $\tilde{\tau}\tilde{\nu}$. As shown in Fig. 5, the $H^\pm \rightarrow \tilde{t}\tilde{b}$ process is not kinematically allowed in CMSSM, while it is open in NMSSM and UMSSM. However, the large top-quark background significantly suppresses such processes. On the other hand, the $H^\pm \rightarrow \tilde{\tau}\tilde{\nu}$ process is possible in all models. Moreover, since it happens through the leptonic

processes, the signal could be clear for such decay processes. The minimum and maximum rates for various decay modes of the charged Higgs boson obtained in the parameter scan are represented in Table III. The values have been chosen as to be consistent with all the constraints applied. As mentioned before, the dominant decay channel, $H^\pm \rightarrow t\bar{b}$, does not leave too much space for the other modes in CMSSM, while it is possible to realize this decay mode as low as a few percent, and these models can significantly yield other decay modes such as those with neutralino and chargino, stop and bottom, and/or stau and neutralino, which can be as high as about 30% in NMSSM and UMSSM. In addition, the decay processes including other Higgs bosons can be also available in the latter models. For instance, NMSSM allows the process, $H^\pm \rightarrow A_1^0 W^\pm$ up to 43%, while the $H^\pm \rightarrow H_2^0 W^\pm$ process can be also realized up to 16%. The latter process is also allowed in UMSSM up to about 30%.

VI. CONCLUSION

We perform numerical analyses for the CMSSM, NMSSM and UMSSM to probe the allowed mass ranges for the charged Higgs boson and its possible decay modes as well as showing the allowed parameter spaces of these models. Since there is no charged scalar in SM, the charged Higgs boson can signal the new physics as well as being distinguishable among the models beyond SM. Throughout our analyses, we find that it is possible to realize much heavier scales ($\gtrsim 10$ TeV) in the NMSSM and UMSSM framework. In addition to the charged Higgs boson, we find $m_{\tilde{t}} \gtrsim 2$ TeV in CMSSM, while it can be as light as about 1 TeV in NMSSM and 500 GeV in UMSSM. These bounds on the stop mass mostly arise from the 125 GeV Higgs boson mass constraint, while this constraint is rather relaxed in NMSSM and UMSSM because of extra contributions from the new sectors in these models. Besides, the sbottom mass cannot be lighter than about 2 TeV in CMSSM and 1 TeV in NMSSM and UMSSM. Such masses for the stop and sbottom exclude $H^\pm \rightarrow \tilde{t}\tilde{b}$ in CMSSM, while it can still be open in NMSSM and UMSSM. Another pair of supersymmetric particles relevant to the charged Higgs boson decay modes is $\tilde{\tau}$ and $\tilde{\nu}$, whose masses are

TABLE III. Minimum and maximum rates for various decay modes of the charged Higgs boson obtained in the parameter scan. The values have been chosen so as to be consistent with all the constraints applied.

Parameters	CMSSM		NMSSM		UMSSM	
	Min (%)	Max (%)	Min (%)	Max (%)	Min (%)	Max (%)
$\text{BR}(H^\pm \rightarrow \tilde{\chi}_1^0 \tilde{\chi}_1^\pm)$...	0.5	...	20	...	23
$\text{BR}(H^\pm \rightarrow \tilde{\chi}_2^0 \tilde{\chi}_1^\pm)$	3	...	1
$\text{BR}(H^\pm \rightarrow \tilde{\chi}_3^0 \tilde{\chi}_1^\pm)$	24	...	21
$\text{BR}(H^\pm \rightarrow \tilde{\chi}_4^0 \tilde{\chi}_1^\pm)$	26	...	25
$\text{BR}(H^\pm \rightarrow \tilde{\chi}_5^0 \tilde{\chi}_1^\pm)$	25	...	19
$\text{BR}(H^\pm \rightarrow \tilde{\chi}_6^0 \tilde{\chi}_1^\pm)$	8
$\text{BR}(H^\pm \rightarrow \tilde{\tau}\tilde{\nu})$...	13	...	33	...	5
$\text{BR}(H^\pm \rightarrow \tilde{t}\tilde{b})$	35	...	8
$\text{BR}(H^\pm \rightarrow A_1^0 W^\pm)$	43
$\text{BR}(H^\pm \rightarrow H_2^0 W^\pm)$	16	...	2
$\text{BR}(H^\pm \rightarrow ZW^\pm)$	3	...	2
$\text{BR}(H^\pm \rightarrow tb)$	73	83	7	95	8	98
$\text{BR}(H^\pm \rightarrow \tau\nu)$...	16	...	17	...	18

bounded as $m_{\tilde{\tau}} \gtrsim 500$ GeV and $m_{\tilde{\nu}} \gtrsim 1$ TeV. Even though their total mass is close by the charged Higgs boson mass, there might be a small window which allows $H^\pm \rightarrow \tilde{\tau}\tilde{\nu}$. We also present the masses for the chargino and neutralino, since the charged Higgs boson can, in principle, decay into them.

While the heavy mass scales in NMSSM and UMSSM open more decay modes for the charged Higgs boson, its heavy mass might be problematic in its production processes. We list the possible production channels and their ranges. The production channels, in which the charged Higgs boson is produced associated with top quark, provide the most promising channels. Considering the same mass scale ($m_{H^\pm} \sim 2$ TeV) in all the models CMSSM and UMSSM predict $\sigma(pp \rightarrow tH^\pm) \sim 10^{-5}$ pb, while NMSSM prediction is one magnitude larger ($\sim 10^{-4}$ pb). Similarly UMSSM prediction fades away as $\sigma(pp \rightarrow t\bar{b}H^\pm) \sim 10^{-7}$ pb, which is much lower than the CMSSM prediction ($\sim 10^{-5}$ pb), while NMSSM yields $\sigma(pp \rightarrow t\bar{b}H^\pm) \sim 10^{-2}$ pb. Even though NMSSM predictions come forward in the charged Higgs predictions, UMSSM allows lighter charged Higgs mass solutions ($m_{H^\pm} \sim 500$ GeV) as well, and such solutions yield much larger production cross section as $\sigma(pp \rightarrow tH^\pm) \sim 10^{-2}$ pb and $\sigma(pp \rightarrow t\bar{b}H^\pm) \sim 10^{-3}$ pb.

Even if these predictions for the charged Higgs boson production are low in comparison to the SM-like Higgs boson, it can be attainable with larger center of mass energy and luminosity. In addition, its decay modes are completely distinguishable from any neutral scalar, and hence it can manifest itself through some decay processes. The dominant decay mode for the charged Higgs boson in CMSSM is mostly to tb with $70\% \lesssim \text{BR}(H^\pm \rightarrow tb) \lesssim 80\%$, while it

is also possible to realize $H^\pm \rightarrow \tau\nu$ and $H^\pm \rightarrow \tilde{\tau}\tilde{\nu}$ up to about 20%. On the other hand, the allowed heavy mass scales in NMSSM and UMSSM allow the modes $H^\pm \rightarrow \tilde{t}\tilde{b}, \tilde{\tau}\tilde{\nu}, \tilde{\chi}_i^\pm \tilde{\chi}_j^0$ in addition to those realized in the CMSSM framework. Among these modes, even though the $\tilde{t}\tilde{b}$ channel distinguishes these models from CMSSM, the large irreducible top-quark background can suppress such processes; thus, it is not easy to probe the charged Higgs boson through such a decay mode. Nevertheless, despite the clear leptonic background, NMSSM and UMSSM imply similar predictions for the $\tilde{\tau}\tilde{\nu}$ decay mode to the results from CMSSM. This channel can probe the charged Higgs in future collider experiments but it cannot distinguish the mentioned SUSY models. On the other hand, $H^\pm \rightarrow \tilde{\chi}_i^\pm \tilde{\chi}_j^0$ is excluded by the current experimental constraints in the CMSSM framework, while it is still possible to include this decay mode in NMSSM and UMSSM. Such decay modes can be probed in the collider experiments through the missing energy and CP -violation measurements. Additionally, the lightest chargino mass in NMSSM and UMSSM is bounded from below as $m_{\tilde{\chi}_1^\pm} \gtrsim 1$ TeV, which seems testable in the near future LHC experiments through the analyses for the chargino-neutralino production processes.

ACKNOWLEDGMENTS

This work was supported by Balikesir University Research Project Grants No. BAP-2017/142 and No. BAP-2017/174. The work of L. S. is supported in part by Ankara University-BAP under Grant No. 17B0443004.

-
- [1] E. Gildener, Gauge symmetry hierarchies, *Phys. Rev. D* **14**, 1667 (1976); Gauge symmetry hierarchies revisited, *Phys. Lett. B* **92**, 111 (1980); S. Weinberg, Gauge hierarchies, *Phys. Lett. B* **82**, 387 (1979); L. Susskind, Dynamics of spontaneous symmetry breaking in the Weinberg-Salam theory, *Phys. Rev. D* **20**, 2619 (1979); M. J. G. Veltman, The infrared-ultraviolet connection, *Acta Phys. Pol. B* **12**, 437 (1981), <http://www.actaphys.uj.edu.pl/fulltext?series=Reg&vol=12&page=437>.
- [2] G. Degrandi, S. Di Vita, J. Elias-Miro, J. R. Espinosa, G. F. Giudice, G. Isidori, and A. Strumia, Higgs mass and vacuum stability in the Standard Model at NNLO, *J. High Energy Phys.* **08** (2012) 098; F. Bezrukov, M. Y. Kalmykov, B. A. Kniehl, and M. Shaposhnikov, Higgs boson mass and new physics, *J. High Energy Phys.* **10** (2012) 140; D. Buttazzo, G. Degrandi, P. P. Giardino, G. F. Giudice, F. Sala, A. Salvio, and A. Strumia, Investigating the near-criticality of the Higgs boson, *J. High Energy Phys.* **12** (2013) 089.
- [3] H. E. Haber, When are radiative corrections important in the minimal supersymmetric model?, in *the 23rd Eloisatron workshop on properties of SUSY particles, Erice, 1992*, arXiv:hep-ph/9305248, pp. 321–372, Conference: C92-09-28.
- [4] V. Khachatryan *et al.* (CMS Collaboration), Search for neutral MSSM Higgs bosons decaying to a pair of tau leptons in pp collisions, *J. High Energy Phys.* **10** (2014) 160.
- [5] S. R. Choudhury and N. Gaur, Dileptonic decay of B(s) meson in SUSY models with large tan Beta, *Phys. Lett. B* **451**, 86 (1999); K. S. Babu and C. F. Kolda, Higgs Mediated $B^0 \rightarrow \mu^+\mu^-$ in Minimal Supersymmetry, *Phys. Rev. Lett.* **84**, 228 (2000).
- [6] R. Aaij *et al.* (LHCb Collaboration), First Evidence for the Decay $B_s^0 \rightarrow \mu^+\mu^-$, *Phys. Rev. Lett.* **110**, 021801 (2013).
- [7] G. Buchalla, A. J. Buras, and M. E. Lautenbacher, Weak decays beyond leading logarithms, *Rev. Mod. Phys.* **68**, 1125 (1996).

- [8] M. Frank and I. Turan, CP asymmetry in charged Higgs decays to chargino-neutralino, *Phys. Rev. D* **76**, 076008 (2007).
- [9] S. P. Martin, A supersymmetry primer, *Adv. Ser. Dir. High Energy Phys.* **21**, 1 (2010); **18**, 1 (1998).
- [10] S. Heinemeyer, O. Stal, and G. Weiglein, Interpreting the LHC Higgs search results in the MSSM, *Phys. Lett. B* **710**, 201 (2012); A. Arbey, M. Battaglia, A. Djouadi, F. Mahmoudi, and J. Quevillon, Implications of a 125 GeV Higgs for supersymmetric models, *Phys. Lett. B* **708**, 162 (2012).
- [11] R. D. Peccei and H. R. Quinn, Constraints imposed by CP conservation in the presence of instantons, *Phys. Rev. D* **16**, 1791 (1977); CP Conservation in the Presence of Instantons, *Phys. Rev. Lett.* **38**, 1440 (1977).
- [12] K. Hagiwara *et al.* (Particle Data Group), Review of particle physics, *Phys. Rev. D* **66**, 010001 (2002).
- [13] C. Panagiotakopoulos and K. Tamvakis, Stabilized NMSSM without domain walls, *Phys. Lett. B* **446**, 224 (1999); New minimal extension of MSSM, *Phys. Lett. B* **469**, 145 (1999); C. Panagiotakopoulos and A. Pilaftsis, Higgs scalars in the minimal nonminimal supersymmetric standard model, *Phys. Rev. D* **63**, 055003 (2001); A. Dedes, C. Hugonie, S. Moretti, and K. Tamvakis, Phenomenology of a new minimal supersymmetric extension of the standard model, *Phys. Rev. D* **63**, 055009 (2001).
- [14] U. Ellwanger, C. Hugonie, and A. M. Teixeira, The next-to-minimal supersymmetric Standard Model, *Phys. Rep.* **496**, 1 (2010); M. Maniatis, The next-to-minimal supersymmetric extension of the Standard Model reviewed, *Int. J. Mod. Phys. A* **25**, 3505 (2010); O. Stal and G. Weiglein, Light NMSSM Higgs bosons in SUSY cascade decays at the LHC, *J. High Energy Phys.* **01** (2012) 071.
- [15] M. Drees, Supersymmetric models with extended Higgs sector, *Int. J. Mod. Phys. A* **04**, 3635 (1989); S. F. King and P. L. White, Nonminimal supersymmetric Higgs bosons at LEP-2, *Phys. Rev. D* **53**, 4049 (1996).
- [16] D. A. Demir, G. L. Kane, and T. T. Wang, The minimal $U(1)'$ extension of the MSSM, *Phys. Rev. D* **72**, 015012 (2005); S. M. Barr, Effects of Extra Light Z Bosons in Unified and Superstring Models, *Phys. Rev. Lett.* **55**, 2778 (1985); J. L. Hewett and T. G. Rizzo, Low-energy phenomenology of superstring inspired $E(6)$ models, *Phys. Rep.* **183**, 193 (1989); M. Cvetič and P. Langacker, Implications of Abelian extended gauge structures from string models, *Phys. Rev. D* **54**, 3570 (1996); G. Cleaver, M. Cvetič, J. R. Espinosa, L. L. Everett, and P. Langacker, Intermediate scales, μ parameter, and fermion masses from string models, *Phys. Rev. D* **57**, 2701 (1998); Classification of flat directions in perturbative heterotic superstring vacua with anomalous $U(1)$, *Nucl. Phys.* **B525**, 3 (1998); D. M. Ghilencea, L. E. Ibanez, N. Irges, and F. Quevedo, TeV scale Z -prime bosons from D-branes, *J. High Energy Phys.* **08** (2002) 016; S. F. King, S. Moretti, and R. Nevzorov, Theory and phenomenology of an exceptional supersymmetric standard model, *Phys. Rev. D* **73**, 035009 (2006); R. Diener, S. Godfrey, and T. A. W. Martin, Discovery and identification of extra neutral gauge bosons at the LHC, [arXiv:0910.1334](https://arxiv.org/abs/0910.1334); P. Langacker, The physics of heavy Z' gauge bosons, *Rev. Mod. Phys.* **81**, 1199 (2009); M. Frank, L. Selbuz, L. Solmaz, and I. Turan, Higgs bosons in supersymmetric $U(1)'$ models with CP violation, *Phys. Rev. D* **87**, 075007 (2013); M. Frank, L. Selbuz, and I. Turan, Neutralino and chargino production in $U(1)'$ at the LHC, *Eur. Phys. J. C* **73**, 2656 (2013); D. A. Demir, M. Frank, L. Selbuz, and I. Turan, Scalar neutrinos at the LHC, *Phys. Rev. D* **83**, 095001 (2011); P. Athron, D. Harries, and A. G. Williams, Z' mass limits and the naturalness of supersymmetry, *Phys. Rev. D* **91**, 115024 (2015); P. Athron, S. F. King, D. J. Miller, S. Moretti, and R. Nevzorov, The constrained exceptional supersymmetric Standard Model, *Phys. Rev. D* **80**, 035009 (2009); Predictions of the constrained exceptional supersymmetric Standard Model, *Phys. Lett. B* **681**, 448 (2009); Constrained exceptional supersymmetric Standard Model with a Higgs near 125 GeV, *Phys. Rev. D* **86**, 095003 (2012); P. Athron, D. Stockinger, and A. Voigt, Threshold corrections in the exceptional supersymmetric Standard Model, *Phys. Rev. D* **86**, 095012 (2012); P. Athron, M. Mühlleitner, R. Nevzorov, and A. G. Williams, Nonstandard Higgs decays in $U(1)$ extensions of the MSSM, *J. High Energy Phys.* **01** (2015) 153; P. Athron, D. Harries, R. Nevzorov, and A. G. Williams, E_6 Inspired SUSY benchmarks, dark matter relic density and a 125 GeV Higgs, *Phys. Lett. B* **760**, 19 (2016); Dark matter in a constrained E_6 inspired SUSY model, *J. High Energy Phys.* **12** (2016) 128; P. Athron, A. W. Thomas, S. J. Underwood, and M. J. White, Dark matter candidates in the constrained exceptional supersymmetric Standard Model, *Phys. Rev. D* **95**, 035023 (2017); P. Athron, J.-h. Park, T. Steudtner, D. Stöckinger, and A. Voigt, Precise Higgs mass calculations in (non)minimal supersymmetry at both high and low scales, *J. High Energy Phys.* **01** (2017) 079.
- [17] P. Langacker and J. Wang, $U(1)'$ symmetry breaking in supersymmetric E_6 models, *Phys. Rev. D* **58**, 115010 (1998).
- [18] M. Aaboud *et al.* (ATLAS Collaboration), Search for high-mass new phenomena in the dilepton final state using proton-proton collisions at $\sqrt{s} = 13$ TeV with the ATLAS detector, *Phys. Lett. B* **761**, 372 (2016); ATLAS Collaboration, Search for new high-mass phenomena in the dilepton final state using 36.1 fb⁻¹ of proton-proton collision data at $\sqrt{s} = 13$ TeV with the ATLAS detector, Report No. ATLAS-CONF-2017-027.
- [19] Y. Hicyilmaz, L. Solmaz, S. H. Tanyildizi, and C. S. Un, Least fine-tuned $U(1)$ extended SSM, [arXiv:1706.04561](https://arxiv.org/abs/1706.04561).
- [20] See, for instance, S. Khalil and C. S. Un, Muon anomalous magnetic moment in SUSY B-L model with inverse seesaw, *Phys. Lett. B* **763**, 164 (2016); L. Delle Rose, S. Khalil, S. J. D. King, C. Marzo, S. Moretti, and C. S. Un, Naturalness and dark matter properties of the BLSSM, *Proc. Sci.*, DIS2017 (2018) 301 [[arXiv:1706.01301](https://arxiv.org/abs/1706.01301)]; Supersymmetric gauged B-L model of dark matter and fine-tuning, *Proc. Sci.*, EPS-HEP2017 (2017) 067 [[arXiv:1710.01116](https://arxiv.org/abs/1710.01116)].
- [21] L. Delle Rose, S. Khalil, S. J. D. King, C. Marzo, S. Moretti, and C. S. Un, Naturalness and dark matter in the supersymmetric B-L extension of the standard model, *Phys. Rev. D* **96**, 055004 (2017).
- [22] W. Porod, SPHENO, a program for calculating supersymmetric spectra, SUSY particle decays and SUSY particle production at e^+e^- colliders, *Comput. Phys. Commun.* **153**, 275 (2003); W. Porod and F. Staub, SPHENO 3.1: Extensions

- including flavor, CP phases and models beyond the MSSM, *Comput. Phys. Commun.* **183**, 2458 (2012).
- [23] F. Staub, Sarah, [arXiv:0806.0538](https://arxiv.org/abs/0806.0538); Automatic calculation of supersymmetric renormalization group equations and self-energies, *Comput. Phys. Commun.* **182**, 808 (2011).
- [24] J. Hisano, H. Murayama, and T. Yanagida, Nucleon decay in the minimal supersymmetric SU(5) grand unification, *Nucl. Phys.* **B402**, 46 (1993); Y. Yamada, SUSY and GUT threshold effects in SUSY SU(5) models, *Z. Phys. C* **60**, 83 (1993); J. L. Chkareuli and I. G. Gogoladze, Unification picture in minimal supersymmetric SU(5) model with string remnants, *Phys. Rev. D* **58**, 055011 (1998).
- [25] T. E. W. Group (CDF and D0 Collaborations), Combination of CDF and D0 results on the mass of the top quark, [arXiv:0903.2503](https://arxiv.org/abs/0903.2503).
- [26] I. Gogoladze, R. Khalid, S. Raza, and Q. Shafi, Higgs and sparticle spectroscopy with gauge-Yukawa unification, *J. High Energy Phys.* **06** (2011) 117.
- [27] I. Gogoladze, Q. Shafi, and C. S. Un, Higgs boson mass from t - b - τ Yukawa unification, *J. High Energy Phys.* **08** (2012) 028; M. Adeel Ajajib, I. Gogoladze, Q. Shafi, and C. S. Un, A predictive Yukawa unified SO(10) model: Higgs and sparticle masses, *J. High Energy Phys.* **07** (2013) 139.
- [28] L. E. Ibanez and G. G. Ross, $SU(2)_L \times U(1)$ symmetry breaking as a radiative effect of supersymmetry breaking in GUTs, *Phys. Lett. B* **110**, 215 (1982); K. Inoue, A. Kakuto, H. Komatsu, and S. Takeshita, Aspects of grand unified models with softly broken supersymmetry, *Prog. Theor. Phys.* **68**, 927 (1982); Erratum, *Prog. Theor. Phys.* **70**, 330 (1983); L. E. Ibanez, Locally supersymmetric SU(5) grand unification, *Phys. Lett. B* **118**, 73 (1982); J. R. Ellis, D. V. Nanopoulos, and K. Tamvakis, Grand unification in simple supergravity, *Phys. Lett. B* **121**, 123 (1983); L. Alvarez-Gaume, J. Polchinski, and M. B. Wise, Minimal low-energy supergravity, *Nucl. Phys.* **B221**, 495 (1983).
- [29] K. Nakamura (Particle Data Group Collaboration), Review of particle physics, *J. Phys. G* **37**, 075021 (2010).
- [30] G. Belanger, F. Boudjema, A. Pukhov, and R. K. Singh, Constraining the MSSM with universal gaugino masses and implication for searches at the LHC, *J. High Energy Phys.* **11** (2009) 026; H. Baer, S. Kraml, S. Sekmen, and H. Summy, Dark matter allowed scenarios for Yukawa-unified SO(10) SUSY GUTs, *J. High Energy Phys.* **03** (2008) 056.
- [31] K. A. Olive *et al.* (Particle Data Group Collaboration), Review of particle physics, *Chin. Phys. C* **38**, 090001 (2014).
- [32] Y. Amhis *et al.* (Heavy Flavor Averaging Group Collaboration), Averages of B-hadron, C-hadron, and tau-lepton properties as of early 2012, [arXiv:1207.1158](https://arxiv.org/abs/1207.1158).
- [33] D. Asner *et al.* (Heavy Flavor Averaging Group Collaboration), Averages of b-hadron, c-hadron, and tau-lepton Properties, [arXiv:1010.1589](https://arxiv.org/abs/1010.1589).
- [34] G. Hinshaw *et al.* (WMAP Collaboration), Nine-year Wilkinson microwave anisotropy probe (WMAP) observations: Cosmological parameter results, *Astrophys. J. Suppl. Ser.* **208**, 19 (2013).
- [35] P. A. R. Ade *et al.* (Planck Collaboration), Planck 2015 results. XIII. Cosmological parameters, *Astron. Astrophys.* **594**, A13 (2016).
- [36] G. Aad *et al.* (ATLAS Collaboration), Observation and measurement of Higgs boson decays to WW^* with the ATLAS detector, *Phys. Rev. D* **92**, 012006 (2015); Study of (W/Z)H production and Higgs boson couplings using $H \rightarrow WW^*$ decays with the ATLAS detector, *J. High Energy Phys.* **08** (2015) 137.
- [37] S. Chatrchyan *et al.* (CMS Collaboration), Measurement of Higgs boson production and properties in the WW decay channel with leptonic final states, *J. High Energy Phys.* **01** (2014) 096; A. M. Sirunyan *et al.* (CMS Collaboration), Measurements of properties of the Higgs boson decaying into the four-lepton final state in pp collisions at $\sqrt{s} = 13$ TeV, *J. High Energy Phys.* **11** (2017) 047; Constraints on anomalous Higgs boson couplings using production and decay information in the four-lepton final state, *Phys. Lett. B* **775**, 1 (2017).
- [38] F. Domingo and U. Ellwanger, Updated constraints from B physics on the MSSM and the NMSSM, *J. High Energy Phys.* **12** (2007) 090.
- [39] T. Li, S. Raza, and K. Wang, Constraining natural SUSY via the Higgs coupling and the muon anomalous magnetic moment measurements, *Phys. Rev. D* **93**, 055040 (2016).
- [40] G. Aad *et al.* (ATLAS Collaboration), Observation of a new particle in the search for the Standard Model Higgs boson with the ATLAS detector at the LHC, *Phys. Lett. B* **716**, 1 (2012); S. Chatrchyan *et al.* (CMS Collaboration), Observation of a new boson at a mass of 125 GeV with the CMS experiment at the LHC, *Phys. Lett. B* **716**, 30 (2012).
- [41] M. Aaboud *et al.* (ATLAS Collaboration), Search for squarks and gluinos in events with an isolated lepton, jets and missing transverse momentum at $\sqrt{s} = 13$ TeV with the ATLAS detector, *Phys. Rev. D* **96**, 112010 (2017).
- [42] G. Degrossi, S. Heinemeyer, W. Hollik, P. Slavich, and G. Weiglein, Towards high precision predictions for the MSSM Higgs sector, *Eur. Phys. J. C* **28**, 133 (2003).
- [43] B. C. Allanach and A. Voigt, Uncertainties in the lightest CP even Higgs boson mass prediction in the minimal supersymmetric Standard Model: Fixed order versus effective field theory prediction, [arXiv:1804.09410](https://arxiv.org/abs/1804.09410); P. Athron, J. h. Park, T. Stuedtner, D. Stöckinger, and A. Voigt, Precise Higgs mass calculations in (non)minimal supersymmetry at both high and low scales, *J. High Energy Phys.* **01** (2017) 079.
- [44] F. Staub and W. Porod, Improved predictions for intermediate and heavy Supersymmetry in the MSSM and beyond, *Eur. Phys. J. C* **77**, 338 (2017).
- [45] CMS Collaboration, Search for electroweak production of charginos and neutralinos in multilepton final states in pp collision data at $\sqrt{s} = 13$ TeV, Report No. CMS-PAS-SUS-16-039.
- [46] A. M. Sirunyan *et al.* (CMS Collaboration), Search for electroweak production of charginos and neutralinos in WH events in proton-proton collisions at $\sqrt{s} = 13$ TeV, *J. High Energy Phys.* **11** (2017) 029; CMS Collaboration, Search for new physics in final states with two opposite-sign, same-flavor leptons, jets, and missing transverse momentum in pp collisions at $\sqrt{s} = 13$ TeV, Report No. CMS-PAS-SUS-16-034.
- [47] J. Y. Araz, G. Corcella, M. Frank, and B. Fuks, Loopholes in Z' searches at the LHC: Exploring supersymmetric and leptophobic scenarios, *J. High Energy Phys.* **02** (2018) 092.

- [48] D. S. Akerib *et al.* (LUX Collaboration), Results on the Spin-Dependent Scattering of Weakly Interacting Massive Particles on Nucleons from the Run 3 Data of the LUX Experiment, *Phys. Rev. Lett.* **116**, 161302 (2016); E. Aprile *et al.* (XENON Collaboration), Physics reach of the XENON1T dark matter experiment, *J. Cosmol. Astropart. Phys.* **04** (2016) 027; P. L. Brink *et al.* (CDMS-II Collaboration), Beyond the CDMS-II dark matter search: SuperCDMS, econf C041213, 2529 (2004), <http://www.slac.stanford.edu/econf/C041213/papers/2529.PDF>; T. Tanaka *et al.* (Super-Kamiokande Collaboration), An indirect search for WIMPs in the Sun using 3109.6 days of upward-going muons in super-Kamiokande, *Astrophys. J.* **742**, 78 (2011); R. Abbasi *et al.* (IceCube Collaboration), Limits on a Muon Flux from Neutralino Annihilations in the Sun with the IceCube 22-String Detector, *Phys. Rev. Lett.* **102**, 201302 (2009).
- [49] W. B. Atwood *et al.* (Fermi-LAT Collaboration), The Large Area Telescope on the Fermi gamma-ray space telescope mission, *Astrophys. J.* **697**, 1071 (2009); H. Abdallah *et al.* (H.E.S.S. Collaboration), Search for Dark Matter Annihilations Towards the Inner Galactic Halo from 10 Years of Observations with H.E.S.S., *Phys. Rev. Lett.* **117**, 111301 (2016).
- [50] O. Buchmueller, C. Doglioni, and L. T. Wang, Search for dark matter at colliders, *Nat. Phys.* **13**, 217 (2017); A. Basalaev (ATLAS Collaboration), Search for WIMP dark matter produced in association with a Z boson with the ATLAS detector, *Eur. Phys. J. Web Conf.* **164**, 08008 (2017); S. Chatrchyan *et al.* (CMS Collaboration), Search for dark matter and large extra dimensions in monojet events in pp collisions at $\sqrt{s} = 7$ TeV, *J. High Energy Phys.* **09** (2012) 094.
- [51] G. Belanger, F. Boudjema, A. Pukhov, and A. Semenov, MICROMEGAS 2.0: A program to calculate the relic density of dark matter in a generic model, *Comput. Phys. Commun.* **176**, 367 (2007); MICROMEGAS 3: A program for calculating dark matter observables, *Comput. Phys. Commun.* **185**, 960 (2014); MICROMEGAS 4.1: Two dark matter candidates, *Comput. Phys. Commun.* **192**, 322 (2015).
- [52] See for instance, H. E. Haber and G. L. Kane, The search for supersymmetry: Probing physics beyond the Standard Model, *Phys. Rep.* **117**, 75 (1985); W. de Boer, Grand unified theories and supersymmetry in particle physics and cosmology, *Prog. Part. Nucl. Phys.* **33**, 201 (1994); D. I. Kazakov, Introduction to supersymmetry, *Proc. Sci., CORFU2014* (2015) 024.
- [53] I. Gogoladze, R. Khalid, and Q. Shafi, Coannihilation scenarios and particle spectroscopy in $SU(4)_c \times SU(2)_L \times SU(2)_R$, *Phys. Rev. D* **80**, 095016 (2009).
- [54] C. Han, K.-i. Hikasa, L. Wu, J. M. Yang, and Y. Zhang, Status of CMSSM in light of current LHC run-2 and LUX data, *Phys. Lett. B* **769**, 470 (2017); J. C. Costa *et al.*, Likelihood analysis of the sub-GUT MSSM in light of LHC 13-TeV data, *Eur. Phys. J. C* **78**, 158 (2018).
- [55] M. Misiak *et al.*, Estimate of $\mathcal{B}(\bar{B} \rightarrow X_s \gamma)$ at $O(\alpha_s^2)$, *Phys. Rev. Lett.* **98**, 022002 (2007).
- [56] Y. Hiçyılmaz, M. Ceylan, A. Altas, L. Solmaz, and C. S. Un, Quasi-Yukawa unification and fine-tuning in U(1) extended SSM, *Phys. Rev. D* **94**, 095001 (2016).
- [57] A. Cici, Z. Kirca, and C. S. Un, Light stops and fine-tuning in MSSM, *Eur. Phys. J. C* **78**, 60 (2018), and references therein.
- [58] L. Calibbi, A. Mariotti, C. Petersson, and D. Redigolo, Selectron NLSP in gauge mediation, *J. High Energy Phys.* **09** (2014) 133.
- [59] ATLAS Collaboration, Search for charged Higgs bosons in the $H^\pm \rightarrow tb$ decay channel in pp collisions at $\sqrt{s} = 13$ TeV using the ATLAS detector, Report No. ATLAS-CONF-2016-089.
- [60] A. A. Barrientos Bendezu and B. A. Kniehl, $W^\pm H^\mp$ associated production at the large hadron collider, *Phys. Rev. D* **59**, 015009 (1998).
- [61] S. Moretti and K. Odagiri, The phenomenology of $W^\pm H^\mp$ production at the large hadron collider, *Phys. Rev. D* **59**, 055008 (1999).
- [62] See <http://theory.sinp.msu.ru/pukhov/calchep.html>; A. Pukhov, CALCHEP 3.2: MSSM, structure functions, event generation, batches, and generation of matrix elements for other packages, [arXiv:hep-ph/0412191](https://arxiv.org/abs/hep-ph/0412191).
- [63] ATLAS Collaboration, Evidence for the associated production of the Higgs boson and a top quark pair with the ATLAS detector, Report No. ATLAS-CONF-2017-077.
- [64] CMS Collaboration, Search for charged Higgs bosons with the $H^\pm \rightarrow \tau^\pm \nu_\tau$ decay channel in the fully hadronic final state at $\sqrt{s} = 13$ TeV, Report No. CMS-PAS-HIG-16-031; M. Aaboud *et al.* (ATLAS Collaboration), Search for charged Higgs bosons produced in association with a top quark and decaying via $H^\pm \rightarrow \tau \nu$ using pp collision data recorded at $\sqrt{s} = 13$ TeV by the ATLAS detector, *Phys. Lett. B* **759**, 555 (2016); ATLAS Collaboration, Report No. ATLAS-CONF-2016-088; V. Khachatryan *et al.* (CMS Collaboration), Search for a charged Higgs boson in pp collisions at $\sqrt{s} = 8$ TeV, *J. High Energy Phys.* **11** (2015) 018.